Master Thesis

Surface plasmon excitation and tunable electromagnetic wave absorption in graphene

Muhammad Shoufie Ukhtary

Department of Physics, Graduate School of Science
Tohoku University

July 2015

Acknowledgments

Alhamdulillah. In this opportunity, I would like to acknowledge everyone who has supported me in finishing my master course and this thesis. First, I would like to say my thanks to Saito-sensei for his assistance and guidance not only on finishing my master course, but also on helping me living my life in Japan. He taught me not only how to be a good scientist, but also how to be a good presenter, which is an important quality of scientist. Also, I will never forget his kindness on taking care of me when I was hospitalized. My special thanks I address to my parents and family for them have given me a lot of support and advice. They always encourage me to do my best and not to give up. For Hasdeo-san and Nugraha-san, I am extremely grateful for your assistance, advice and support. You are really awesome tutors and friends throughout my ups and downs. For all of my lab mates : Siregar-san, Thomas-san, Pourya-san, Hung-san, Inoue-san, Shirakura-san, Tatsumi-san, Mizuno-san, It has been a great time to work with you all.

Not to forget is my thanks to all 2013 Indonesian IGPAS students : Rais, Rouf, Siregar, Stevanus, Hasan and Intan. You have been a great companions throughout thick and thin. For all of my Indonesian friends that I cannot mention one by one here, I am so thankful to have you all. I consider you as my own brothers and sisters. Thank you for taking care of me in my difficult time. Also, I would like to acknowledge Nicholas for being such good friend and dormmate. Thanks for many interesting and fruitful discussions, I learnt a lot of things from you. And also for Wang and Russel, thanks for being very nice friend and dormmate. I hope we can still live nearby.

The last but not the least, I would like to address my thankfulness to Tohoku University and Japanese Government (MEXT) for giving me the chance to study and to do research in Japan. This has been my unforgetable experience and I am so lucky to have it.

Contents

Chapter 1

Introduction

1.1 Purpose of the study

Graphene, which is a single layer of carbon atom arranged in honeycomb lattice, has attracted a lot of interest because of its peculiar features such as its two-dimensional nature and linear electronic dispersion at so-called Dirac point [1, 2, 3, 4, 5, 6]. This linear behaviour of electronic band structure is different from to electronic band structure of other two-dimensional electron gas, which possesses parabolic electronic band structure. Elementary excitations in graphene have been studied extensively [7, 8, 9, 10, 11, 12, 13, 14, 15, 16, 17, 18, 19, 20] and one of those is plasmon [7, 8, 9, 10, 11, 12, 13]. Plasmon is the quantum of elementary excitation involving collective oscillation of electrons [21]. Plasmon can propagate at certain frequencies and wave vectors [21, 22, 23, 24, 25]. Due to the linear band structure, plasmon properties in graphene are different from the ones in normal two-dimensional electron gas, too [7, 26, 22]. The plasmon in graphene has been studied extensively theoretically and also experimentally. Because of its two-dimensional nature, graphene plasmon is categorized as surface plasmon (**SP**).

Graphene is also well-known as transparent material. On undoped condition, graphene absorbs only around 2.3% incident Electromagnetic (EM) wave [4, 27, 28, 6]. This property is important for making device such as optical devices such as liquid-crystal displays, touch screen and light-emitting diodes [4, 27, 28]. However, other devices such as solar cells, photodectors and optical antennas require a strong optical

absorption. The purpose of this thesis is to explain the properties of graphene SP, which includes the study of SP dispersion relation and damping. Another purpose is to get a tuneable high absorption of EM wave by graphene. This contains the study of EM wave absorption by graphene and the relation to SP excitation. We consider that graphene placed between two dielectric media can be a good geometry for discussing EM absorption.

Theoretically, graphene plasmon can be studied by using random phase approximation (RPA) [7, 26, 22, 24] which is used to calculate the dielectric function of a material. To observe plasmon experimentally, electron energy loss spectroscopy (EELS) is used [21, 29]. Both theoretical and experimental studies can result the dispersion relation of plasmon [7, 26, 30, 31] that is the relation between plasmon frequency and wave vector. The theoretical dispersion relation of graphene SP can be calculated by using RPA theory of quantum mechanics or by solving Maxwell equations on the surface (semiclassical model) [7, 13]. Those two methods agree with each other up to a limit of wave vector ($q \to 0$). The dielectric function can be related to conductivity. Conductivity is used to study the absorption of EM wave. It will be shown in this thesis that the real part of conductivity is related to the absorption.

This master thesis is organized as follows: In the remaining part of Chapter 1, the background for understanding this thesis is given. In Chapter 2, the electronic properties of graphene and RPA theory of dielectric function are reviewed. The dielectric function is used to explain SP in Chapter 3 and also to derive the conductivity in Chapter 4. In Chapter 3, the graphene SP properties is presented. In Chapter 4, EM wave absorption by graphene and its relation to SP excitation are explained. In Chapter 5, we provide the conclusion of this thesis.

1.2 Background

Here we show the basic concepts which are important for understanding this thesis.

1.2.1 Absorption of light by graphene

Graphene is well-known as a transparent material [27, 28]. It transmits almost all visible light and its transmittance can be expressed in terms of the fine-structure

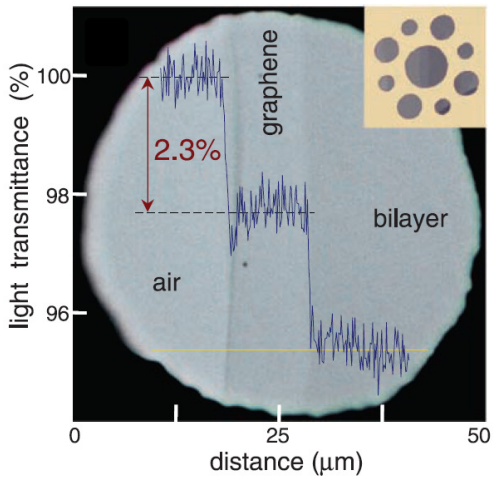

Figure 1.1 Graphene transparency. An aperture partially covered by single layer graphene in the middle and bilayer graphene in right side. The plot shows the transmittance of visible light [27].

constant $\alpha = e^2/\hbar c$ [27, 28]. This transmittance can be expressed as below [27, 28],

$$T \approx 1 - \pi\alpha = 97.7\% \tag{1.1}$$

Single layer graphene only reflects negligible portion of incident light, around $< 0.1\%$ of incident light [27, 28]. This will give 2.3% absorption of single layer graphene for visible light. This absorption characteristic is due to graphene's universal conductivity $\sigma_0 = e^2/4\hbar$ [28]. This has already been proved experimentally and the absorption increases linearly with the increase of layer's number [27, 28]. Fig. 1.1 shows the absorption of visible light by single layer graphene and bilayer graphene [27]. It can be seen that the absorption is proportional to number of graphene layers [27, 28]. It is reported also that optical spectroscopy shows the absorption independent of wavelength [27]. This dependency of graphene optical properties which only depend on fundamental constant is due to the two-dimensional nature and gapless electronic dispersion of graphene [27].

Due to its optical properties, graphene has several applications. The high transparency of graphene can be useful for designing optical devices such as liquid-crystal displays, touch screen and LED [28, 32, 33, 34, 35]. However, other devices such as

Fig. 1.1: Fig/fig1k4.eps

solar cells, photodectors and optical antennas require a strong optical absorption in order to generate a large photocurrent [28]. In recent years, the possibilities of enhancing optical absorption in graphene have been studied extensively, but most of them utilize complicated techniques such as using a grating coupler or shaping the graphene into rib-bons or disks [8, 36, 37]. Practical optoelectronic applications of graphene are thus still challenging.

1.2.2 Surface plasmon in material and its usage

Before going to plasmon, we need to define what plasma is. A plasma is a medium with equal concentration of positive and negative charges, of which at least one charge type is mobile. In a solid (for example metal) the negative charges of the conduction electrons are balanced by an equal concentration of positive charge of the ion cores. This conduction electrons can oscillate about positive charges and this oscillation is called plasma oscillation. The quantum of plasma oscillation is called plasmon. More formal definition of plasmon is the quantum of elementary excitation involving collective oscillation of electron [21]. There are two kinds of plasmon, first kind is the bulk plasmon and the second kind is the surface plasmon [21]. The bulk plasmon differs from surface plasmon in their dimensionality and polarization. The bulk plasmon is the oscillation of three-dimensional (3D) electron gas which occurs inside the material, while surface plasmon oscillation is confined within two-dimension (2D) surface of material. The polarization of bulk plasmon is longitudinal, while surface plasmon's is tranversal. The illustrations for both bulk plasmon and SP are shown in Fig. 1.2.

To get the idea of this kind of charge oscillation, we take an example of bulk plasmon in a solid. In Fig. 1.3, the electrons are indicated by the gray background, while the positive ion cores are indicated by the + sign. The positive ion cores are immobile. If, for example, we apply an external electric field $\mathbf{E}$, this will make electrons displaced by amount of displacement u as depicted in Fig. 1.3(b). If we release the electrons by turning off the external electric field, we can have oscillation of these electrons about positive ion cores. This can be pictured by imagining that the gray background is going up and down in oscillatory manner (Fig. 1.3(d)). A collective displacement of the electron cloud by distance u creates a surface charge density $\sigma = \pm neu$ at the slab boundaries (Fig. 1.3(c)). This leads to a homogenous electric

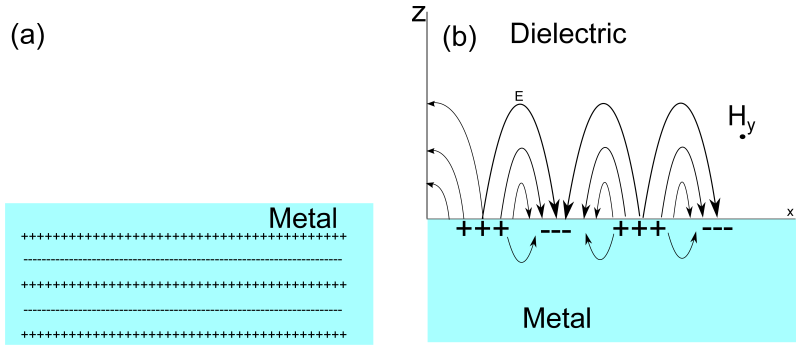

Figure 1.2 (a) Illustration of bulk plasmon. The negative charge (electrons) inside metal oscillate about fixed positive charge. (b) Illustration of surface plasmon. The negative charge (electrons) oscillate about fixed positive charge on surface of metal. The lines are the accompanying electric fields.

field inside slab which will act as a restoring force of the electrons. The equation of motion of u in a unit volume of the electron gas with concentration n is [21, 38]

$$\frac{d^2u}{dt^2} + \omega_p u = 0 \qquad , \tag{1.2}$$

where ω_p is expressed by

$$\omega_p = \sqrt{\frac{ne^2}{\varepsilon_0 m}} \quad . \tag{1.3}$$

This clearly shows the oscillatory motion of electrons of frequency ω_p. This natural frequency is called as bulk plasmon frequency.

Here assume that all electrons move in phase. Therefore, the ω_p only corresponds to limit wave vector k equal to zero. A bulk plasmon of small wave vector has a frequency approximately the frequency equal to ω_p. However, if the correction of wave vector dependency is also considered, the wave vector dependency on frequency of oscillation can be written as follows [21, 38]

$$\omega \approx \omega_p(1 + 3k^2 v_{\mathrm{F}}/10\omega_p^2 + ...) \quad , \tag{1.4}$$

where v_{F} is the Fermi velocity. Due to the longitudinal nature of excitation, bulk plasmon do not couple to transverse electromagnetic waves, and can only be excited

Fig. 1.2: Fig/fig1k6.eps
Fig. 1.3: Fig/fig1k7.eps

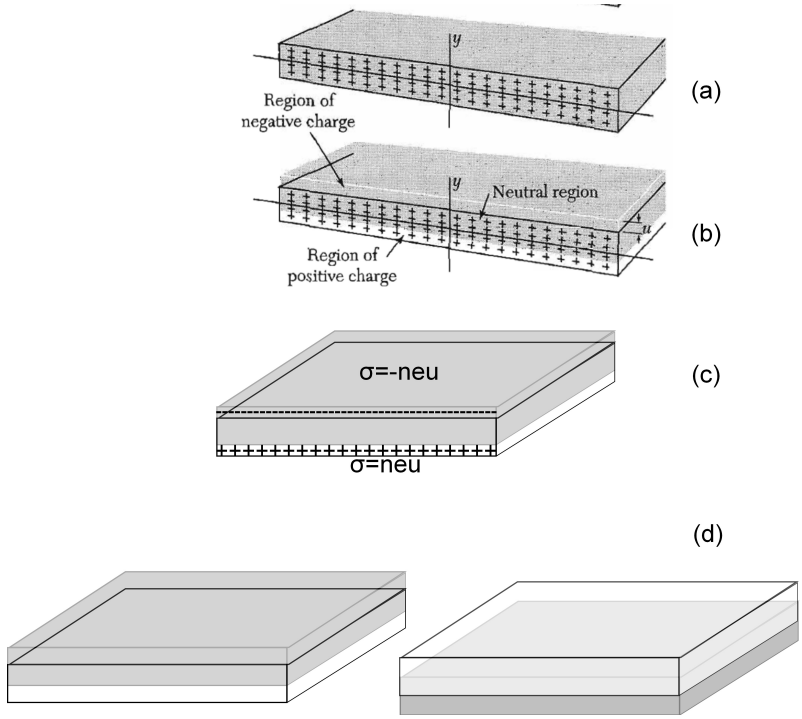

Figure 1.3 (a) Neutral slab, with a unit volume of the electron gas is indicated by gray background and positive ion cores by + sign. (b) Electrons are displaced with distance u. (c) Displacing electrons leads to surface density $\sigma = \pm neu$ which will create electric field inside the slab. The electric field acts as restoring force. (d) Illustration of bulk plasmon, the gray slab goes up and down [21, 38].

by the impact of particle. Thus in order to observe this kind of excitation, electron energy loss spectroscopy is adopted in experiments [21, 29]. For metal, when high energy electrons are passed through thin metallic foils, the loss of electrons energy gives information of ω_p and k. For most metals, ω_p is within ultraviolet regime in order of 5 - 15 eV. This depends also on details of energy band structure of an electron [21].

Even though bulk plasmon cannot couple to transverse electromagnetic waves, the frequency of bulk plasmon ω_p is important as a threshold frequency for external electromagnetic wave propagating through the plasma. If the frequency of electromagnetic wave is less than ω_p, the electrons can follow the EM wave to screen out the incident field, and thus the EM does not propagate, instead it will be reflected. Of course the electromagnetic wave can enter the plasma up to some distance, this distance is known as a skin depth. If the frequency of electromagnetic wave is more than ω_p, the

electrons cannot respond fast enough to screen the incident field. The wave will be transmitted.

SP is essentially an electromagnetic wave that is trapped on the surface because of their interaction with free electrons of the conductor [39]. In this interaction, the free electrons respond collectively by oscillating in resonance with the external electromagnetic wave. The work on SP field was pioneered by Ritchie in the 1950s, who predicted the existence of self-sustained collective excitations at metal surface [40]. In this pioneering work, he predicted theoretically that a fast electron fired at thin metal foil acquired a new lowered loss due to the collective excitation on the surface [40]. Later on, the electron energy loss experiments conducted by Powell and Swan proved the existence of surface excitation of electrons, and now it is called surface plasmon [21, 41].

Fig. 1.4 shows the electron energy loss spectra for aluminium and magnesium [21].

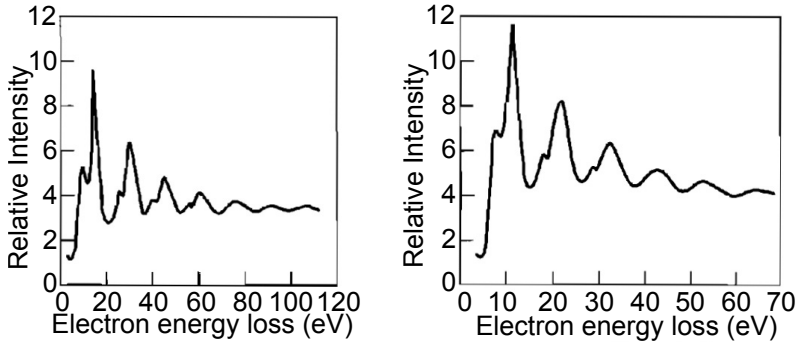

Figure 1.4 Electron energy loss spectra for (a) aluminium and (b) magnesium with primary electron energies 2020eV. There are 12 loss peaks and 10 loss peaks for aluminum and magnesium, respectively. These loss peaks are made up of combinations of 10.3 and 15.3 eV losses for aluminium and 7.1 and 10.6 eV losses for magnesium. The lower losses are due to surface plasmon, while the higher ones are due to bulk plasmon [21, 41]

.

In both spectra, the loss peaks are made up of combinations of two kinds of loss. The higher energy losses are due to bulk plasmon, while the lower ones are due to surface plasmon. This proves the existence of collective excitation on the surface, which has been predicted theoretically by Ritchie before.

An important point for SP is that SP has transverse polarization. Therefore, it

Fig. 1.4: Fig/fig1k1.eps
Fig. 1.5: Fig/fig1k8.eps

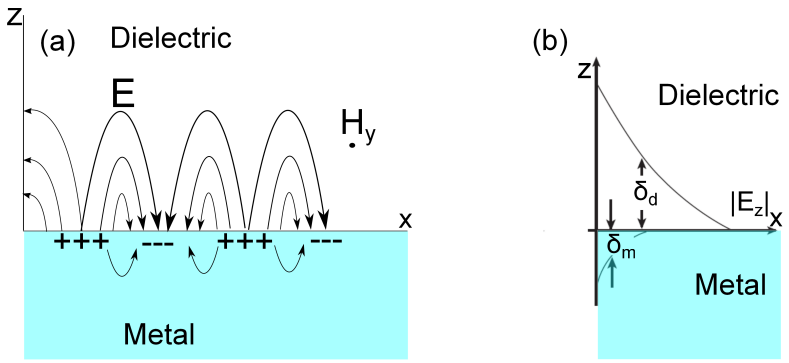

Figure 1.5 (a)Illustration of surface plasmon. (b) The evanescent field of SP [39].

can be excited by external electromagnetic wave. SP has an essentially transverse magnetic character as shown in Fig. 1.5(a). The field component perpendicular to the surface becomes enhanced near the surface and decays exponentially with distance away from the surface. The field in this perpendicular direction is an evanescent wave. The decay length of the field inside dielectric material above the metal, denoted by δ_d in Fig. 1.5(b) is of the order of half the wavelength of electromagnetic wave involved in the excitation, while the decay length inside the metal, denoted by δ_m corresponds to skin depth of metal. The field does not propagate away from the surface, which means that SP is bounded within the surface and non-radiative [39].

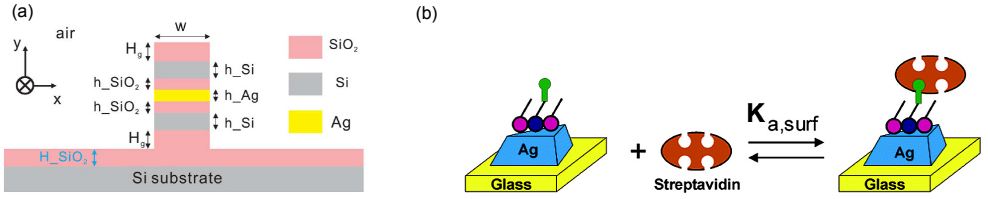

Figure 1.6 Plasmonic devices (a) Plasmonic waveguide [42] and (b) Plasmonic biosensor [43]

.

The rise of surface plasmon science has allowed the emergence of new field of technology, so-called plasmonics [38, 39, 44, 45]. In plasmonics, the applications of surface plasmon are explored [38, 39, 44, 45]. The ability of surface plasmon to be tuned and localized at nano scale gives rise to rapid development of surface plasmon

Fig. 1.6: Fig/fig1k2.eps

based device, such as nano scale circuits that have ability to carry optical signals and electric currents, the plasmonic waveguide at subwavelength [46], electro-plasmon modulator [43] and plasmon based bio sensor [42]. Plasmonics is also considered to be a practicable way to control light at nano scale [13]. Fig. 1.6 shows some plasmonic device. In Fig. 1.6(a), we have plasmonic waveguide, which is silicon-based 3-D hybrid wave guide to guide SP on surface of silver (Ag). This consists of three layers of ($SiO_2-Si-SiO_2$) placed on both sides of a thin silver film with a symmetry. It is predicted that it is capable of guiding with nanometric confinement and long propagation distance (around 696 μm) [42]. Fig. 1.6(b) shows plasmonic biosensor. It uses triangular silver nanoparticles to support localized SP. It is found that the process of SP excitation is unexpectedly sensitive to nanoparticle size, shape (triangle), and local ($10-30$ nm) external dielectric environment. This sensitivity to the nanoenvironment can be utilized to develop a new class of nanoscale affinity biosensors [43].

1.2.3 Graphene as plasmonic material

Graphene has been discussed by many researchers in plasmonic field as a potential plasmonic material. Some theoretical researches to predict the existence of SP on graphene has been conducted by researchers [7, 47, 12, 26, 13]. One of the important results is done by Hwang and Das Sarma [7]. They predicted theoretically the existence of SP on graphene by plotting its dispersion relation (Fig. 1.7). The dispersion relation relates frequency and wave vector of a SP. They predicted that graphene SP can exist in any wave length, even though it is damped. The damped SP is shown as dispersion line inside single particle excitation (SPE) in Fig. 1.7. SPE in Fig. 1.7 depicts the energy dissipation of system for exciting an electron as interband and intraband (SPE_{inter} and SPE_{intra}) transitions by the Coloumb interaction.

It is predicted that graphene has the ability to support surface plasmon within terahertz (THz) frequency [13, 48, 49]. This frequency range is important for technological application, for instance, plasmonic terahertz sources [13], amplifier [11, 12], antenna [50, 12], graphene-based plasmonic wave guide [10, 12, 51] and graphene plasmonic metamaterial [51, 12]. Fig. 1.8 shows the application of graphene SP. Fig. 1.8(a) they proposed graphene dipole plasmonic antenna which works at THz frequency

Fig. 1.7: Fig/fig1k5.eps

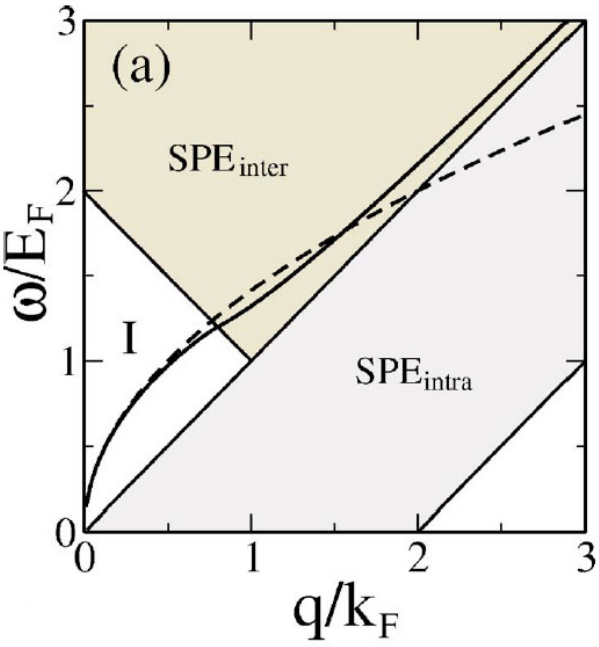

Figure 1.7 Grapehe SP dispersion relation [7]. Background lattice dielectric constant is 2.5

range [50]. Graphene here acts as dipole-like antenna and each dipole arm is a set of two stacked graphene patches separated by a thin Al_2O_3 insulating film used to control graphene complex conductivity via electrostatic field effect. The antenna exploits dipole-like plasmonic resonances that can be frequency-tuned on large range via the electric field effect in a graphene stack. The silicone here acts as lens for better directivity [50]. In Fig. 1.8(b) graphene plasmonic waveguide is shown. This device has enabled us to guide EM wave at $f = 30$THz (Infrared). The waveguide shown here also includes the ability to split the wave propagation direction by proper design of conductivity patterns on the graphene by using uneven ground plane which will make the bias electric field distributed spatially [51].

The most important property of graphene SP is the easy tunability of graphene SP due to an easy control of carriers densities by electrical gating and doping [9, 12]. The SP in graphene are also reported to have a relatively low loss compared with conventional plasmonic materials [13, 12], notably metals which are reported to have

Fig. 1.8: Fig/fig1k3.eps

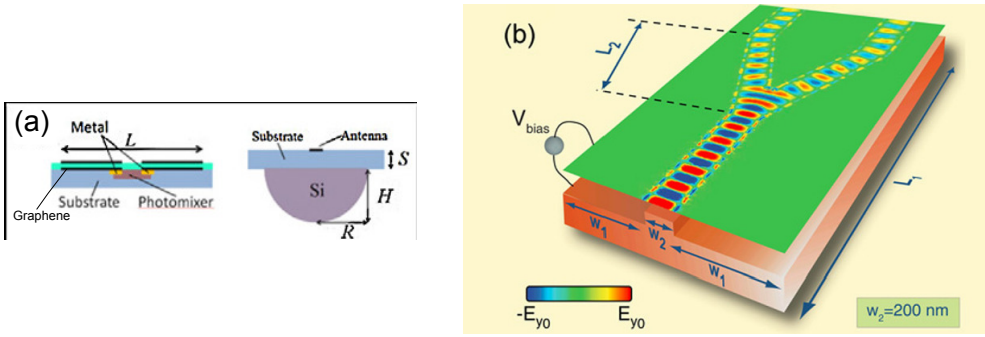

Figure 1.8 Plasmonic devices (a) Graphene dipole plasmonic antenna [50] and (b) Graphene plasmonic waveguide [51]. The green layer is graphene.

enormous losses. The loss here is related to propagation length of the SP. Another important property of graphene SP is the high confinement compared to metals [12]. This is important parameter of plasmonic materials which describes the ability of a material to confine light and is characterized by vertical decay length. Both of propagation and vertical length of graphene SP are tunable by doping [12]. This low loss and high confinement properties are useful for developing applications in subwavelength optics [12]. Graphene, due to its flexibility, also supports the propagation of SP along flexible and curved surface [12].

Chapter 2

Electronic Properties of Graphene

In this chapter, the electronic properties of graphene will be reviewed. These electronic properties include the electronic structure of graphene and also the dielectric function. First, the electronic structure of graphene is derived by using simple tight binding (STB) model. We focus on the electronic structure near the Dirac point (K-point). After getting the electronic structure of graphene, the general formulation of the dielectric function is derived by using the RPA theory. The electronic structue of graphene will be used for obtaining the dielectric function of graphene.

2.1 Electronic structure of graphene

2.1.1 Graphene unit cell and Brillouin zone

Graphene is a planar allotrope of carbon where all the carbon atoms form covalent bonds in a single plane [1, 2, 3, 4, 5, 6]. It has a honeycomb lattice structure. This lattice structure of graphene has been observed experimentally [2] and is shown by Figure 2.1(a). The covalent bond between nearest neighbor carbon atoms is called σ-bond, which are the strongest type of covalent bond among the materials [2, 52]. The σ-bond has the electrons localized along the plane connecting two carbon atoms and are responsible for the great strength and mechanical properties of graphene [2].

Graphene is well-knows as the mother of three carbon allotropes [2, 3]. Several layers of graphene sheets are stacked together by the van der Waals force to form three dimensional (3D) graphite, while by wrapping it up, a 0D fullerene can be made

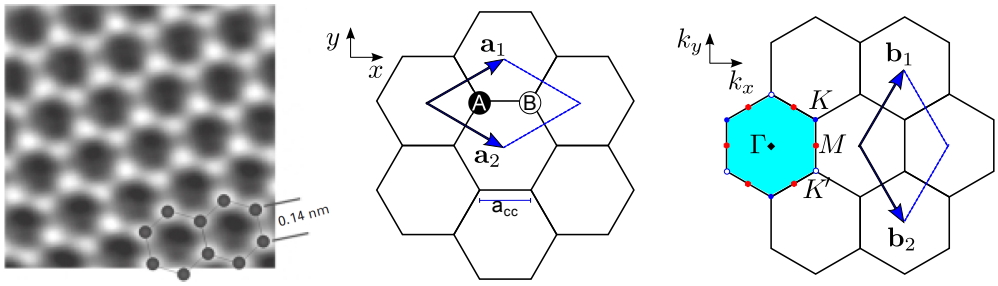

Figure 2.1 (a) Graphene hexagonal lattice observed experimentally by transmission electron aberration-corrected microscope (TEAM) [2]. It is shown that carbon-carbon distance is 0.142 nm. (b) The graphene unit cell consisting of two atomic sites A and B. $\mathbf{a_1}$ and $\mathbf{a_2}$ are the unit vectors and $\mathbf{a}_{cc}$ is the nearest neighbor carbon-carbon distance. (b) Brillouin zone of graphene (shaded hexagon). $\Gamma, \mathrm{K}, \mathrm{K}'$, and M denoted by a closed diamond, closed circles, opened circles, and closed hexagons, respectively, are the high symmetry points. $\mathbf{b_1}$ and $\mathbf{b_2}$ are reciprocal lattice vectors [3].

and by rolling it up, a 1D single wall nanotube is made.

The direct lattice and unit cell of graphene are shown by Figure 2.1(b). The unit vectors of graphene can be expressed by

$$\mathbf{a_1} = \left(\frac{\sqrt{3}}{2}, \frac{1}{2}\right) a, \quad \mathbf{a_2} = \left(\frac{\sqrt{3}}{2}, -\frac{1}{2}\right) a. \tag{2.1}$$

$a = \sqrt{3}a_{cc}$ is the lattice constant of graphene unit cell and $a_{cc} = 0.142$ nm is the distance between two carbon atoms as shown by Figure 2.1(a) and (b).

Figure 2.1(c) shows the reciprocal lattice of graphene, which is hexagonal lattice, but rotated 90° with respect to the direct lattice. The first Brillouin zone area is the shaded hexagon which is enclosed by reciprocal lattice vectors. The reciprocal lattice vectors are given by

$$\mathbf{b_1} = \left(\frac{1}{\sqrt{3}}, 1\right) \frac{2\pi}{a}, \quad \mathbf{b_2} = \left(\frac{1}{\sqrt{3}}, -1\right) \frac{2\pi}{a}. \tag{2.2}$$

The high symmetry points are denoted by circles in Figure 2.1(c). These high symmetry points are defined at the center Γ, the center of an edge M, and the hexagonal corners K and K' of the Brillouin zone. The position of the M and K point can be described with respect of Γ point by vectors

$$\Gamma\mathrm{M} = \frac{2\pi}{a}\left(\frac{1}{\sqrt{3}}, 0\right), \quad \Gamma\mathrm{K} = \frac{2\pi}{a}\left(\frac{1}{\sqrt{3}}, 3\right), \tag{2.3}$$

Fig. 2.1: Fig/fig2k1.eps

with $|\Gamma M| = 2\pi/\sqrt{3}a$, $|\Gamma K| = 4\pi/3a$ and $|MK| = 2\pi/3a$. There are six K points (including K′ points) and six M points within the Brillouin zone.

2.1.2 Electronic structure of graphene

The electronic energy dispersion of graphene is calculated by using simple tight binding (STB) model [1, 3]. The electronic energy dispersion describes the energy E as a function of wave vector $\mathbf{k}$. In the tight binding approximation, the eigenfunctions of electrons are made up by the Bloch function that consists of the to atomic orbitals.

In graphene, the valence orbitals (2s, $2p_x$, $2p_y$) are hybridized to one another and form σ-bonds, while $2p_z$ orbital gives a π bond. The $2p_z$ forms the π band independently from σ bands and the π band lies around the Fermi energy. Hence, the electronic transport and optical properties of graphene originate mainly from the π band [2, 3]. Therefore, hereafter we adopt the STB method to model the π band.

The wave function of an electron in graphene can be written as a linear combination of the atomic orbitals

$$\Psi(\mathbf{k},\mathbf{r}) = C_A(\mathbf{k})\phi_A(\mathbf{k},\mathbf{r}) + C_B(\mathbf{k})\phi_B(\mathbf{k},\mathbf{r}), \tag{2.4}$$

where $\phi(\mathbf{k},\mathbf{r})$ is the Bloch wave function. The $C_j \quad (j = A, B)$ is the coefficient of Bloch wave function . This Bloch wave function consists of the linear combination of atomic orbital, that is $2p_z$ orbital. The Bloch wave function can be written as

$$\phi_j(\mathbf{k},\mathbf{r}) = \frac{1}{\sqrt{N}} \sum_{\mathbf{R_j}}^{N} e^{i\mathbf{k}\cdot\mathbf{R_j}} \varphi(\mathbf{r} - \mathbf{R_j}). \quad (j = A \text{ or } B) \tag{2.5}$$

where $\mathbf{R_A}$ and $\mathbf{R_B}$ are the position of A and B sites, respectively. The electronic energy dispersion $E(\mathbf{k})$ is obtained by minimizing

$$E(\mathbf{k}) = \frac{\langle\Psi|H|\Psi\rangle}{\langle\Psi|\Psi\rangle}, \tag{2.6}$$

in respect to wave function coefficients . Inserting electron wave function to Eq.(2.6), a secular equation is obtained [1]

$$\sum_{j'} H_{jj'} C_{j'}(\mathbf{k}) = E \sum_{j'} S_{jj'} C_{j'}(\mathbf{k}) \quad (j, j' = A, B), \tag{2.7}$$

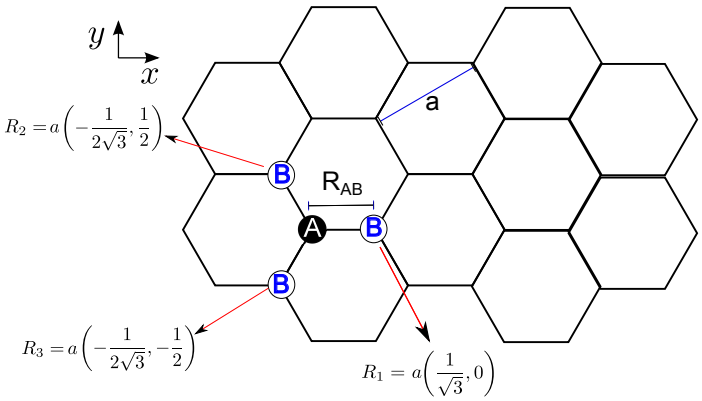

Figure 2.2 The reference atomic site is A. The 3 nearest neighbors (B atomic site) are shown. The positions of nearest neighbors are indicated by R_1, R_2, and R_3 with respect to A site.

where $H_{\mathrm{j}j'} = \langle\phi|H|\psi\rangle$ and $S_{\mathrm{j}j'} = \langle\phi|\psi\rangle$ are called the transfer integral matrix and the overlap integral matrices [1]. Then, Eq. (2.7) has turned into eigenvalue problem, where it can be written explicitly as

$$\begin{pmatrix} H_{\mathrm{A}A}(\mathbf{k}) & H_{\mathrm{A}B}(\mathbf{k}) \\ H_{\mathrm{B}A}(\mathbf{k}) & H_{\mathrm{B}B}(\mathbf{k}) \end{pmatrix} \begin{pmatrix} C_{\mathrm{A}}(\mathbf{k}) \\ C_{\mathrm{B}}(\mathbf{k}) \end{pmatrix} = E(\mathbf{k}) \begin{pmatrix} S_{\mathrm{A}A}(\mathbf{k}) & S_{\mathrm{A}B}(\mathbf{k}) \\ S_{\mathrm{B}A}(\mathbf{k}) & S_{\mathrm{B}B}(\mathbf{k}) \end{pmatrix} \begin{pmatrix} C_{\mathrm{A}}(\mathbf{k}) \\ C_{\mathrm{B}}(\mathbf{k}) \end{pmatrix} . \tag{2.8}$$

Thus, the electron energy dispersion can be obtained by solving the secular equation

$$det\,[\mathbf{H} - E\mathbf{S}] = 0 \quad . \tag{2.9}$$

To solve Eq. (2.9), we need to evaluate the matrix elements of transfer matrix and overlap matrix. First, we evaluate the matrix elements of transfer matrix. By using Bloch wave function in Eq. (2.5),

$$\begin{aligned} H_{\mathrm{A}A} &= \frac{1}{N} \sum_{\mathbf{R_A}, \mathbf{R'_A}} e^{i\mathbf{k}\cdot(\mathbf{R_A} - \mathbf{R'_A})} \left\langle \varphi(\mathbf{r} - \mathbf{R'_A}) | H | \varphi(\mathbf{r} - \mathbf{R_A}) \right\rangle \\ &= \varepsilon_{2\mathrm{p}} + (\text{terms equal to or more distant than } \mathbf{R_A} = \mathbf{R'_A} \pm \boldsymbol{a_i}). \end{aligned} \tag{2.10}$$

The high order contribution to $H_{\mathrm{A}A}$ can be neglegted. Therefore, the value of $H_{\mathrm{A}A}$ gives $\varepsilon_{2\mathrm{p}}$, which is the energy of the 2p orbital of a carbon atom. By using the same calculation, $H_{\mathrm{A}A}$ also gives $\varepsilon_{2\mathrm{p}}$. As for off-diagonal elements of the transfer matrix,

Fig. 2.2: Fig/fig2k2.eps

the same method is used. Here, the largest contribution comes from three nearest neighbor atoms and we can neglect more distant terms. The three nearest neighbors as we can see in Fig. 2.2. The off-diagonal elements can be written as

$$\begin{aligned} H_{\mathrm{AB}} &= \frac{1}{N}\sum_{\mathbf{R_A},\mathbf{R_i}} e^{i\mathbf{k}\cdot(\mathbf{R_i})}\left\langle\varphi(\mathbf{r}-\mathbf{R'_A})|H|\varphi(\mathbf{r}-\mathbf{R_A}-\boldsymbol{R_i})\right\rangle \ (i=1,...3) \\ &\equiv tf(\mathbf{k}) \quad , \end{aligned} \tag{2.11}$$

where $\left\langle\varphi(\mathbf{r}-\mathbf{R'_A})|H|\varphi(\mathbf{r}-\mathbf{R_A}-\boldsymbol{R_i})\right\rangle$ denotes contribution of each nearest neighbor atom, denoted by t. By inserting the coordinates of the nearest neighbor atoms, $f(\mathbf{k})$ in Eq. (2.11)can be evaluated

$$\begin{aligned} f(\mathbf{k}) &= \sum_{\mathbf{R_i}} e^{i\mathbf{k}\cdot\mathbf{R_i}} \quad (i=1,...3) \\ &= e^{ik_x a/\sqrt{3}} + 2e^{-ik_x a/2\sqrt{3}}\cos(\frac{k_y a}{2}). \end{aligned} \tag{2.12}$$

The transfer matrix is a Hermite matrix, so $H_{BA}(\mathbf{k}) = H^*_{AB}(\mathbf{k})$. Now we have a complete transfer matrix. The remaining problem is to evaluate the overlap integral matrix. The overlap of same atomic site is 1, $H_{AA}(\mathbf{k}) = H_{BB}(\mathbf{k}) = 1$, while off-site one should be calculated by considering only the nearest neigbors

$$\begin{aligned} H_{\mathrm{AB}} &= \frac{1}{N}\sum_{\mathbf{R_A},\mathbf{R_i}} e^{i\mathbf{k}\cdot(\mathbf{R_i})}\left\langle\varphi(\mathbf{r}-\mathbf{R'_A})|\varphi(\mathbf{r}-\mathbf{R_A}-\boldsymbol{R_i})\right\rangle \ (i=1,...3) \\ &= sf(\mathbf{k}), \end{aligned} \tag{2.13}$$

where $\left\langle\varphi(\mathbf{r}-\mathbf{R'_A})|\varphi(\mathbf{r}-\mathbf{R_A}-\boldsymbol{R_i})\right\rangle$ denotes contribution of each neighbor atom, denoted by s. This matrix is also a Hermite matrix, $S_{BA}(\mathbf{k}) = S^*_{AB}(\mathbf{k})$.

After getting all necessary matrices, the electronic energy dispersion can be calculated by Eq. (2.9). The solution is

$$E^{\pm}(\mathbf{k}) = \frac{\mp tw(\mathbf{k})}{1 \mp sw(\mathbf{k})} \quad , \tag{2.14}$$

where we set $\varepsilon_{2\mathrm{p}} = 0$. The value of t = -3.033 eV and s = 0.129. $+(-)$ sign denotes the π (π^*) band, with negative value of t. Hereafter, they will be called valence and conduction band, respectively. The electronic energy dispersion of graphene is plotted in Fig. 2.3.

Fig. 2.3: Fig/fig2k3.eps

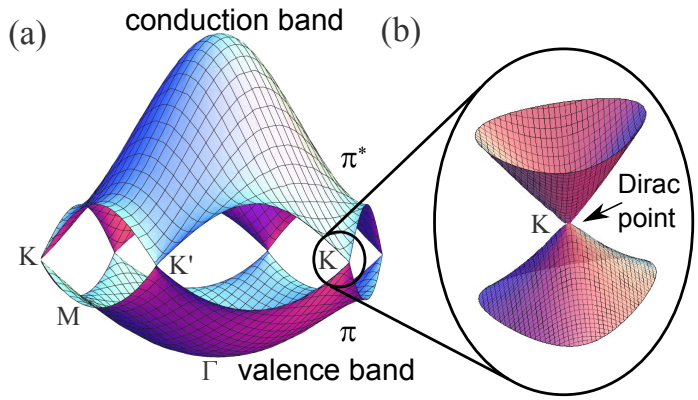

Figure 2.3 (a) The electronic energy dispersion of graphene throughout the whole region of Brillouin zone. (b) The dispersion around K point [3].

Since there are two π electrons per unit cell, the two electrons fully occupy the valence band. The conduction band and valence band are degenerate at the K points at which the Fermi energy exists. This degenerated point is also called as Dirac point. For small wave vector $\mathbf{k}$ measured from K point, $f(\mathbf{k})$ can be expanded around this point and the electronic energy dispersion around this point can be obtained. With $\mathbf{k} = (k_x, k_y)$ measured from a K point, the electronic energy dispersion in the vicinity of the K points reads

$$E^{\pm}(\mathbf{k}) = \pm\frac{\sqrt{3}at}{2}\sqrt{k_x^2 + k_y^2} \quad , \tag{2.15}$$

which shows linear behavior to $|\mathbf{k}|$ as shown in Fig. 2.3(b). This linear dispersion is often called Dirac cone. On Dirac cone, one can write the effective Hamiltonian as

$$\begin{aligned} H^K(\mathbf{k}) &= \begin{pmatrix} 0 & \hbar v_{\mathrm{F}}(k_x - ik_y) \\ \hbar v_{\mathrm{F}}(k_x + ik_y) & 0 \end{pmatrix} \\ &= \hbar v_{\mathrm{F}}|\mathbf{k}| \begin{pmatrix} 0 & e^{-i\theta_k} \\ e^{i\theta_k} & 0 \end{pmatrix}, \end{aligned} \tag{2.16}$$

where $v_{\mathrm{F}} = \frac{\sqrt{3}}{2}\frac{at}{\hbar} \approx 10^6\,\mathrm{m/s}$ is the Fermi velocity at Dirac cone and θ_k is angle between $\mathbf{k}$ to x-axis $\tan\theta_k = \frac{k_y}{k_x}$. The corresponding eigenvectors for positive energies (electrons) can be written as

$$\Psi_+^K(\mathbf{k}, r) = \tfrac{1}{\sqrt{2}} e^{i\mathbf{k}\cdot\mathbf{r}} \begin{pmatrix} e^{-i\theta_k/2} \\ e^{i\theta_k/2} \end{pmatrix} = e^{i\mathbf{k}\cdot\mathbf{r}} \left|+, k\right\rangle, \tag{2.17}$$

and for negative energies (holes) as

$$\Psi_{-}^{K}(\mathbf{k},r)=\tfrac{1}{\sqrt{2}}e^{i\mathbf{k}\cdot\mathbf{r}}\begin{pmatrix} e^{-i\theta_k/2} \\ -e^{i\theta_k/2} \end{pmatrix}=e^{i\mathbf{k}\cdot\mathbf{r}}\left|-,k\right\rangle, \tag{2.18}$$

2.2 Graphene dielectric function

After obtaining the electronic energy dispersion relation of graphene, we will use this dispersion to obtain another electronic property of graphene, the dielectric function. Dielectric function is considered as a measure of electric response when a perturbation is applied to a system. In this section, we are going to explain how to derive the expression of a general dielectric function and adopt it to for graphene as system. Based on the results of this section, SP dispersion can be obtained, which will be presented in Chapter 3. Dielectric function of graphene will also be used to determine the conductivity of graphene, which will be used to calculate absorption probability of EM wave in Chapter 4.

2.2.1 General random phase approximation (RPA) dielectric function

When an external electric field is applied to a system consisting of electrons, the system will respond as a perturbation by rearranging the electrons, so that it can screen the applied field. In many cases, the response of the system is linear response of the applied field [24]. Such consideration is well-known as linear response theory. The response of the system due to the applied field can be depicted by its susceptibility, which is related to dielectric function. The dielectric function as function of wave vector q and frequency ω is given by the ratio of Fourier components of external potential to total potential of the system or equivalently the ratio of the Fourier component of external charge density to total charge density as follows,

$$\frac{\varphi_{\text{ext}}}{\varphi}=\frac{\rho_{\text{ext}}^{e}}{\rho^{e}}=\varepsilon(q,\omega) \quad . \tag{2.19}$$

The total charge density ρ^e is the summation of external charge density and induced charge density $\rho^e=\rho^e_{\text{ext}}+\rho^e_{\text{ind}}$, here ρ is defined particle density. The relation between them is $\rho^e = e\rho$. The induced charge density can be obtained by using the linear

response theory. In the linear response theory, the change of expectation value of an observable due to perturbation can be expressed by [24] :

$$\delta \langle O \rangle = -i \int \theta(t-t') \left\langle \left[\hat{O}(r,t), \hat{H}'(r',t') \right] \right\rangle dt' \quad . \tag{2.20}$$

Eq. (2.20) is the popular Kubo formula [24]. The average $\langle\rangle$ is taken with respect to unperturbed Hamiltonian. H' is a perturbing Hamiltonian acting on the system at position r' and time t', which affects the observable O measured at position r and time t. For electric field as perturbing field and the O in this section is charge density. In particular the induced charge is the change of charge density. The perturbing Hamiltonian is written as $H'(r',t') = \int e\rho(r',t')\varphi_{\text{ext}}(r',t')dr'$, then the induced charge is expressed as follows :

$$\rho_{\text{ind}}(r,t) = -ie \int dr' \int \theta(t-t') \langle [\hat{\rho}(r,t), \hat{\rho}(r',t')] \rangle \varphi_{\text{ext}}(r',t')dt' \quad . \tag{2.21}$$

Here we assume that the system is translation-invariant and we introduce the electric susceptibility or polarization function $\Pi(r-r', t-t') = -i\theta(t-t') \langle [\hat{\rho}(r,t), \hat{\rho}(r',t')] \rangle$, we arrive at the Fourier component of induced charge density obtained by convoluting.

$$\begin{aligned} \rho_{\text{ind}}(r,t) &= e \int dr' \int \Pi(r-r', t-t') \varphi_{\text{ext}}(r',t')dt' \\ &\downarrow \qquad\qquad \text{Convolution} \\ \rho_{\text{ind}}(q,\omega) &= e\ \Pi^e(q,\omega)\varphi_{\text{ext}}(q,\omega) \quad . \end{aligned} \tag{2.22}$$

The Fourier transform of external potential can be expressed by [24],

$$\varphi_{ext}(q,\omega) = \frac{e}{4\pi\varepsilon_0}\ \mathcal{F}(\frac{1}{|r-r'|})\rho_{\text{ext}}(q,\omega) \quad , \tag{2.23}$$

where $\mathcal{F}(\frac{1}{|r-r'|})$ is the Fourier transform of $\frac{1}{|r-r'|}$. Using Eq. (2.22), (2.23) and (2.19), we can obtain the dielectric function as follows,

$$\varepsilon(q,\omega) = \frac{1}{1+v(q)\Pi^e(q,\omega)} \quad , \tag{2.24}$$

where $v(q) = \frac{e^2}{4\pi\varepsilon_0}\mathcal{F}(\frac{1}{|r-r'|})$ is Fourier transform of Coloumb potential.

To evaluate the polarization, the concept of second quantization is employed [24]. The density operator $\rho = \sum_k c_k^\dagger(t)c_{k+q}(t)$ and Hamiltonian $H = \sum_k \epsilon_k c_k^\dagger c_k$ are used and it implies that we should work in q space. Plugging the operator to polarization

expression and taking derivative for polarization with respect to time t, we arrive at following equation [24]:

$$i\frac{\partial}{\partial t}\Pi_{0k} = \delta(t-t')\left(n_k - n_{k+q}\right) + \left(\epsilon_{k+q} - \epsilon_k\right)\Pi^e_{0k} \quad , \tag{2.25}$$

where n_k is occupation number defined as $n_k = \left\langle c_k^\dagger c_k \right\rangle$ and $\Pi_0 = \frac{1}{V}\sum_k \Pi_{0k}$, where V is volume. Π_{0k} is the polarization function for one electron wave vector k. Fourier transforming the both side of Eq. (2.25) with respect to time and solving for Π_0, we arrive at expression for non-interacting polarization [24].

$$\Pi_0(q,\omega) = \frac{1}{V}\sum_k \frac{n_k - n_{k+q}}{\hbar\omega + \epsilon_k - \epsilon_{k+q} + i\eta} \quad . \tag{2.26}$$

Eq. (2.26) is called non-interacting polarization function because the Hamiltonian used in calculation does not contain the interaction between two electrons, hence it contains only kinetic energy in ϵ_k. To include the interaction between electrons, the Hamiltonian must contain interaction term

$$V_{\text{int}} = \frac{1}{2}\sum_{kk'q\neq 0} v(q) c^\dagger_{k+q} c^\dagger_{k'-q} c_{k'} c_k \quad . \tag{2.27}$$

Thus $H = \sum_k \epsilon_k c_k^\dagger c_k + \frac{1}{2}\sum_{kk'q\neq 0} v(q) c^\dagger_{k+q} c^\dagger_{k'-q} c_{k'} c_k$. Using the same derivation of Eq. (2.25) once again, but now taking into account the interaction term, we will arrive at following equation [24],

$$i\frac{\partial}{\partial t}\Pi_k = \delta(t-t')\left(n_k - n_{k+q}\right) - i\theta\left(t-t'\right)\left\langle\left[-\left[H, c_k^\dagger c_{k+q}\right], \rho_{-q}\right]\right\rangle \quad . \tag{2.28}$$

Now the random phase approximation (RPA) comes into a play when we evaluate the commutator containing V_{int} [24],

$$\begin{aligned}
\left[V_{\text{int}}, c_k^\dagger c_{k+q}\right] =& \frac{1}{2}\sum_{k',k'',q'\neq 0} v(q')\left(c^\dagger_{k'+q'} c^\dagger_{k''-q'} c_{k''}\left[c_{k'}, c_k^\dagger c_{k+q}\right]\right. \\
&+ c^\dagger_{k'+q'} c^\dagger_{k''-q'}\left[c_{k''}, c_k^\dagger c_{k+q}\right] c_{k'} + c'_{k'+q}\left[c_{k''-q'}, c_k^\dagger c_{k+q}\right] c_{k''} c_{k'} \\
&\left. + \left[c^\dagger_{k'+q'}, c_k^\dagger c_{k+q}\right] c_{k''-q'} c_{k'}\right) \\
=& \frac{1}{2}\sum_{k',q'\neq 0} v(q')\left(c^\dagger_{k+q'} c^\dagger_{k'-q'} c_{k'} c_{k+q} + c^\dagger_{k'+q'} c^\dagger_{k-q'} c_{k+q} c_{k'}\right. \\
&\left. - c^\dagger_{k'+q'} c^\dagger_k c_{k+q+q'} c_{k'} - c^\dagger_k c^\dagger_{k'-q'} c_{k'} c_{k+q-q'}\right) \quad .
\end{aligned} \tag{2.29}$$

In RPA, we replace the pairs of operators with their mean-field expression, which is their average values.

$$\begin{aligned}\left[V_{\text{int}}, c_k^\dagger c_{k+q}\right] \approx & \frac{1}{2}\sum_{k',q'\neq 0} v(q')\Big(c_{k+q'}^\dagger c_{k+q}\left\langle c_{k'-q'}^\dagger c_{k'}\right\rangle + \left\langle c_{k+q'}^\dagger c_{k+q}\right\rangle c_{k'-q'}^\dagger c_{k'} \\ & + c_{k-q'}^\dagger c_{k+q}\left\langle c_{k'+q'}^\dagger c_{k'}\right\rangle + \left\langle c_{k-q'}^\dagger c_{k+q}\right\rangle c_{k'+q'}^\dagger c_{k'} \\ & - c_{k'+q'}^\dagger c_{k'}\left\langle c_k^\dagger c_{k+q+q'}\right\rangle - \left\langle c_{k'+q'}^\dagger c_{k'}\right\rangle c_k^\dagger c_{k+q+q'} \\ & - c_k^\dagger c_{k+q-q'}\left\langle c_{k'-q'}^\dagger c_{k'}\right\rangle - \left\langle c_k^\dagger c_{k+q-q'}\right\rangle c_{k'-q'}^\dagger c_{k'}\Big) \\ = & v(q)\left(n_{k+q}-n_k\right)\sum_{k'} c_{k'-q}^\dagger c_{k'} \quad . \end{aligned} \tag{2.30}$$

Eq. (2.28) can be evaluated. By going to frequency domain for Eq. (2.28), we have

$$(\hbar\omega + \epsilon_k - \epsilon_{k+q})\Pi_k = (n_k - n_{k+q})(1 + v(q)\sum_{k'}\Pi_{k'}) \quad . \tag{2.31}$$

The interacting polarization can be solved

$$\begin{aligned}\Pi(q,\omega) &= \frac{1}{V}\sum_k \frac{n_k - n_{k+q}}{\hbar\omega + \epsilon_k - \epsilon_{k+q} + i\eta}\left(1 + v(q)\Pi(q,\omega)\right) \\ \Pi(q,\omega) &= \Pi_0(q,\omega)\left(1 + v(q)\Pi(q,\omega)\right) \quad ,\end{aligned}$$

which gives

$$\Pi(q,\omega) = \frac{\Pi_0(q,\omega)}{1 - v(q)\Pi_0(q,\omega)} \quad . \tag{2.32}$$

By Eq. (2.32), the interacting polarization is expressed in term of non-interacting polarization. This is the result of RPA approximation. Inserting the interacting polarization expression Eq. (2.32) to Eq. (2.24), we arrive at the general RPA dielectric function

$$\varepsilon(q,\omega) = 1 - v(q)\Pi_0(q,\omega) \quad . \tag{2.33}$$

2.2.2 Graphene dielectric function

From the previous discussion, the general RPA dielectric function has been obtained. In this section, we are going to calculate the dielectric function for graphene. To do that, we need to calculate the non-interacting polarization of graphene, hereafter we denote it by $\Pi_{0g}(q,\omega)$, which is given by Eq. (2.34). For first case, the non-interacting polarization of undoped graphene will be calculated [23]. Undoped means that the

Fermi energy is exactly at Dirac point and that all electrons occupies the valence band. More explanations of the derivation can be seen in Appendix A.

$$\Pi_{0g}(q,\omega) = \frac{4}{A}\sum_{k} \frac{n_k - n_{k+q}}{\hbar\omega + \epsilon_k - \epsilon_{k+q} + i\eta} |\langle sk|s'k+q\rangle|^2 \quad , \tag{2.34}$$

where A is the area of graphene. We use an area A instead of V in Eq. (2.34), because graphene is two-dimensional material. We evaluate $\Pi_{0g}(q,\omega)$ only at K-point, where two bands (conduction and valence) touch each other at the Dirac point. The factor 4 in Eq. (2.34) comes from spin and valley degeneracy. Since we have two different energy bands, there will be an overlap of wave function, it is denoted by $F_{ss'} = |\langle sk|s'k+q\rangle|^2$ [23], where s is the band index whose value is 1(-1) for conduction(valence) band and be denoted by +(-) for conduction(valence) band. The overlap of wave function can be given by using wave function in Eqs. (2.17) and (2.18) [23].

$$\begin{aligned} F_{ss'} =& \frac{1}{4}|e^{i(\theta_k - \theta_{k+q})} + ss'|^2 \\ =& \frac{1}{2}\left(ss'\frac{k+q\cos\phi}{|\mathbf{k}+\mathbf{q}|} + 1\right) \quad , \end{aligned} \tag{2.35}$$

where the angle ϕ is the angle between vector $\mathbf{k}$ and $\mathbf{q}$. The next step is to evaluate the summation in Eq. 2.34. First, the summation over s is carried out.

$$\begin{aligned} \Pi_{0g}(q,\omega) =& \frac{4}{A}\sum_{k} F_{++}\frac{n_{k,+} - n_{k+q,+}}{\hbar\omega + \epsilon_{k,+} - \epsilon_{k+q,+} + i\eta} + F_{-+}\frac{n_{k,-} - n_{k+q,+}}{\hbar\omega + \epsilon_{k,-} - \epsilon_{k+q,+} + i\eta} \\ &+ F_{+-}\frac{n_{k,+} - n_{k+q,-}}{\hbar\omega + \epsilon_{k,+} - \epsilon_{k+q,-} + i\eta} + F_{--}\frac{n_{k,-} - n_{k+q,-}}{\hbar\omega + \epsilon_{k,-} - \epsilon_{k+q,-} + i\eta} \quad . \end{aligned} \tag{2.36}$$

Because undoped condition, we will have only two non-trivial terms

$$\Pi_{0g}(q,\omega) = \frac{4}{A}\sum_{k}\left[\frac{F_{-+}n_{k,-}}{\hbar\omega + \epsilon_{k,-} - \epsilon_{k+q,+} + i\eta} - \frac{F_{+-}n_{k+q,-}}{\hbar\omega + \epsilon_{k,+} - \epsilon_{k+q,-} + i\eta}\right] \quad . \tag{2.37}$$

To simplify the problem, it is easier for consideration to decompose the polarization function into real and imaginary part We first calculate on the imaginary part and then obtain the real part by the Kramers-Kronig relation. Using Eq. (2.35) The imaginary part of polarization can be written as (omitting the negative solution of frequency)

$$\mathrm{Im}\,\Pi_{0g}(q,\omega) = -\frac{2\pi}{A\hbar}\sum_{k}\left(1 - \frac{k+q\cos\phi}{|\mathbf{k}+\mathbf{q}|}\right)\delta(\omega - v_{\mathrm{F}}k - v_{\mathrm{F}}|\mathbf{k}+\mathbf{q}|) \quad . \tag{2.38}$$

Then the summation in Eq. (2.38) is evaluated by transforming it into integral. The integration on ϕ in Eq. (2.38) is changed into on $\cos\phi$ and also the δ-function is also changed in term of $\cos\phi$ by using $\delta(f(x)) = \sum_i \delta(x - x_i)/|\frac{\partial f(x)}{\partial x}|_{x_i}$.

$$\begin{aligned}
\mathrm{Im}\,\Pi_{0g}(q,\omega) &= -\frac{2\pi}{A\hbar}\frac{A}{(2\pi)^2}\int kdk\int d\phi\left(1-\frac{k+q\cos\phi}{|\mathbf{k}+\mathbf{q}|}\right)\delta(\omega - v_{\mathrm{F}}k - v_{\mathrm{F}}|\mathbf{k}+\mathbf{q}|) \\
&= -\frac{1}{\pi\hbar}\int kdk\int\frac{d(\cos\phi)}{\sin\phi}\left(1-\frac{k+q\cos\phi}{|\mathbf{k}+\mathbf{q}|}\right)\frac{|\mathbf{k}+\mathbf{q}|}{v_{\mathrm{F}}kq} \\
&\times\delta(\cos\phi - \frac{\omega^2 - 2v_{\mathrm{F}}k\omega - v_{\mathrm{F}}^2q^2}{2v_{\mathrm{F}}^2kq}) \quad . \qquad (2.39)
\end{aligned}$$

The integration on $\cos\phi$ in Eq. (2.39) is now easy to calculate because of δ-function integration. The simplification of Eq. (2.40) can be seen in Appendix A. Finally we obtain

$$\begin{aligned}
\mathrm{Im}\,\Pi_{0g}(q,\omega) &= -\frac{1}{\pi\hbar}\int dk\frac{v_{\mathrm{F}}^2q^2-(\omega-2v_{\mathrm{F}}k)^2}{v_{\mathrm{F}}\sqrt{(2v_{\mathrm{F}}^2kq)^2-(\omega^2-2v_{\mathrm{F}}k\omega-v_{\mathrm{F}}^2q^2)^2}} \\
&= -\frac{1}{\pi\hbar}\int dk\frac{v_{\mathrm{F}}^2q^2-(\omega-2v_{\mathrm{F}}k)^2}{v_{\mathrm{F}}\sqrt{(v_{\mathrm{F}}^2q^2-(\omega-2v_{\mathrm{F}}k)^2)(\omega^2-v_{\mathrm{F}}q^2)}} \\
&= -\frac{1}{\pi\hbar}\frac{1}{v_{\mathrm{F}}\sqrt{\omega^2-v_{\mathrm{F}}q^2}}\int dk\sqrt{v_{\mathrm{F}}^2q^2-(\omega-2v_{\mathrm{F}}k)^2} \quad . \qquad (2.40)
\end{aligned}$$

Evaluating the integral over k should be done carefully. The limit of integration is determined by the previous $\delta(\cos\phi - \frac{\omega^2-2v_{\mathrm{F}}k\omega-v_{\mathrm{F}}^2q^2}{2v_{\mathrm{F}}^2kq})$. From the δ-function, we will have inequality $-1 \le \frac{\omega^2-2v_{\mathrm{F}}k\omega-v_{\mathrm{F}}^2q^2}{2v_{\mathrm{F}}^2kq} \le 1$. After evaluating the inequality, we get two constraints on the integral : (1) $\frac{\omega}{2v_{\mathrm{F}}} - \frac{q}{2} \le k \le \frac{\omega}{2v_{\mathrm{F}}} + \frac{q}{2}$. (2) $\omega \ge v_{\mathrm{F}}q$. Here, the integration can be performed by substitution of $\omega - 2v_{\mathrm{F}}k = x$.

$$\begin{aligned}
\mathrm{Im}\,\Pi_{0g}(q,\omega) &= -\frac{1}{\pi\hbar}\frac{\theta(\omega-v_{\mathrm{F}}q)}{v_{\mathrm{F}}\sqrt{\omega^2-v_{\mathrm{F}}q^2}}\int_{\frac{\omega}{2v_{\mathrm{F}}}-\frac{q}{2}}^{\frac{\omega}{2v_{\mathrm{F}}}+\frac{q}{2}} dk\sqrt{v_{\mathrm{F}}^2q^2-(\omega-2v_{\mathrm{F}}k)^2} \\
&= -\frac{1}{2\pi\hbar}\frac{\theta(\omega-v_{\mathrm{F}}q)}{v_{\mathrm{F}}\sqrt{\omega^2-v_{\mathrm{F}}q^2}}\left[\frac{1}{2}x\sqrt{v_{\mathrm{F}}^2q^2-x^2}+\frac{1}{2}v_{\mathrm{F}}^2q^2\arcsin\frac{x}{v_{\mathrm{F}}q}\right]_{qv_{\mathrm{F}}}^{-qv_{\mathrm{F}}} \\
&= -\frac{q^2}{4\hbar\sqrt{\omega^2-v_{\mathrm{F}}q^2}}\theta(\omega-v_{\mathrm{F}}q) \quad . \qquad (2.41)
\end{aligned}$$

Imaginary part of polarization is thus obtained in Eq. (2.41). $\theta(x)$ is step function. The real part of Π_{0g} can be calculated by using the Kramers-Kronig relation and the integration can be performed by similiar substitution of Eq. (2.41) .

$$\begin{aligned}\mathrm{Re}\,\Pi_{0g}(q,\omega) &= \frac{2}{\pi}\int_0^\infty \frac{\omega' \mathrm{Im}\,\Pi^e_{0g}(q,\omega')}{\omega'^2-\omega^2}d\omega' \\ &= \left[\frac{2\theta(v_\mathrm{F}q-\omega)}{\sqrt{v_\mathrm{F}^2q^2-\omega^2}}\arctan\frac{\sqrt{x+\omega^2-v_\mathrm{F}^2q^2}}{v_\mathrm{F}^2q^2-\omega^2}\right]_{v_\mathrm{F}^2q^2-\omega^2}^{\infty} \\ &= -\frac{q^2}{4\hbar\sqrt{v_\mathrm{F}q^2-\omega^2}}\theta(v_\mathrm{F}q-\omega) \quad . \end{aligned} \tag{2.42}$$

Finally, we have the complete polarization expression of undoped graphene and also the dielectric function as in Eq. (2.43) $v(q)$ is now $e^2/2\varepsilon_0 q$ for two-dimensional electron gas.

$$\Pi_{0g}(q,\omega) = -\frac{q^2}{4\hbar}\left(\frac{\theta(v_\mathrm{F}q-\omega)}{\sqrt{v_\mathrm{F}q^2-\omega^2}} + i\frac{\theta(\omega-v_\mathrm{F}q)}{\sqrt{\omega^2-v_\mathrm{F}q^2}}\right) \quad . \tag{2.43}$$

Finally we get the dielectric function for undoped graphene.

$$\epsilon(q,\omega) = 1 - \frac{e^2}{2\varepsilon_0 q}\Pi_{0g}(q,\omega) \quad . \tag{2.44}$$

For doped case, Fermi energy is not located at the Dirac point, but at conduction band in the case of electron doping. The electrons partially occupy the conduction band. The electron excitation can be either interband or intraband as shown in Fig. 2.4. In order to calculate the polarization for doped graphene, we are going back to Eq. (2.36) and changing the variable of $ss' = \beta$ and $s = \alpha$, where β is 1(-1) for intraband (interband) transition [53, 7].

$$\Pi^{\alpha\beta}_{0g}(q,\omega) = \frac{2}{A}\sum_{k\alpha\beta}\frac{n_{\alpha,k}-n_{\alpha\beta,k+q}}{\hbar\omega+\alpha(\hbar v_\mathrm{F}k-\hbar v_\mathrm{F}\beta|\mathbf{k}+\mathbf{q}|)+i\eta}\left(1+\beta\frac{k+q\cos\phi}{|\mathbf{k}+\mathbf{q}|}\right) \tag{2.45}$$

The summation is easier to evaluate if we separately consider imaginary and real part. The imaginary part of polarization can be written as

$$\begin{aligned}\Pi^{\alpha\beta}_{0g}(q,\omega) = -\frac{2\pi}{A}\sum_{k\alpha}(n_{\alpha,k}-n_{\alpha\beta,k+q})\left(1+\beta\frac{k+q\cos\phi}{|\mathbf{k}+\mathbf{q}|}\right) \\ \delta(\hbar\omega+\alpha(\hbar v_\mathrm{F}k-\hbar v_\mathrm{F}\beta|\mathbf{k}+\mathbf{q}|)) \quad . \end{aligned} \tag{2.46}$$

Fig. 2.4: Fig/fig2k4.eps

To evaluate the summation, we change it into integration, just like we do before in Eq. (2.39). For interband transition $\beta = -1$, only negative α contributes to the integration, so that we get only positive solution of ω in delta function. For intraband transition $\beta = 1$, only positive α contributes, because for intraband, the contribution of transition within valence band is zero (for $\alpha = -1$, $n_{\alpha,k} - n_{\alpha,k+q} = n_{-,k} - n_{-,k+q} = 0$). The integration on angle is changed to be on $\cos\phi$ and also the δ-function is also changed in term of $\cos\phi$. Afterward, $\mathrm{Im}\,\Pi_{0g}^{\mathrm{intra}}$ and $\mathrm{Im}\,\Pi_{0g}^{\mathrm{inter}}$ denote imaginary part of polarization for intraband and interband transition, respectively and the imaginary part of polarization is $\mathrm{Im}\,\Pi_{0g}(q,\omega) = \mathrm{Im}\,\Pi_{0g}^{\mathrm{intra}} + \mathrm{Im}\,\Pi_{0g}^{\mathrm{inter}}$.

$$\begin{aligned}
\mathrm{Im}\,\Pi_{0g}^{\mathrm{intra}}(q,\omega) =& -\frac{1}{\pi\hbar}\int kdk \int d(\cos\phi)\left(1+\frac{k+q\cos\phi}{|\mathbf{k}+\mathbf{q}|}\right)(n_{+,k}-n_{+,k+q}) \\
& \delta(\cos\phi - \frac{\omega^2 - v_{\mathrm{F}}^2 q^2 + 2v_{\mathrm{F}}k\omega}{2v_{\mathrm{F}}^2 kq})\frac{|\mathbf{k}+\mathbf{q}|}{kqv_{\mathrm{F}}}\frac{2kqv_{\mathrm{F}}^2}{\sqrt{4v_{\mathrm{F}}^4k^2q^2-(\omega^2+2kv_{\mathrm{F}}\omega-q^2)^2}} \\
=& -\frac{1}{\pi\hbar}\frac{1}{v_{\mathrm{F}}\sqrt{v_{\mathrm{F}}^2q^2-\omega}}\int dk\sqrt{(\omega+2kv_{\mathrm{F}})^2 - v_{\mathrm{F}}^2q^2} \qquad (2.47)
\end{aligned}$$

$$\begin{aligned}
\mathrm{Im}\,\Pi_{0g}^{\mathrm{inter}}(q,\omega) =& -\frac{1}{\pi\hbar}\int kdk \int d(\cos\phi)\left(1-\frac{k+q\cos\phi}{|\mathbf{k}+\mathbf{q}|}\right)(n_{-,k}-n_{+,k+q}) \\
& \delta(\cos\phi - \frac{\omega^2 - v_{\mathrm{F}}^2 q^2 - 2v_{\mathrm{F}}k\omega}{2v_{\mathrm{F}}^2 kq})\frac{|\mathbf{k}+\mathbf{q}|}{kqv_{\mathrm{F}}}\frac{2kqv_{\mathrm{F}}^2}{\sqrt{4v_{\mathrm{F}}^4k^2q^2-(\omega^2-2kv_{\mathrm{F}}\omega-q^2)^2}} \\
=& -\frac{1}{\pi\hbar}\frac{1}{v_{\mathrm{F}}\sqrt{\omega-v_{\mathrm{F}}^2q^2}}\int dk\sqrt{v_{\mathrm{F}}^2q^2 - (\omega+2kv_{\mathrm{F}})^2} \qquad (2.48)
\end{aligned}$$

The remaining integration is now on k. Here we need to determine the boundary of integration. For the interband transition, the constraints of k and ω come from the energy condition of interband transition ($\hbar v_{\mathrm{F}}|\mathbf{k}+\mathbf{q}| > E_{\mathrm{F}}$) and together with the

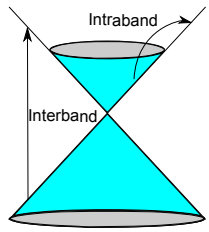

Figure 2.4 Electron transition near K-point. The interband and intraband transition are shown.

condition of delta function $\delta(\cos\phi - \frac{\omega^2 - v_F^2 q^2 + 2v_F k\omega}{2v_F^2 kq})$ for the wave vector. We will obtain three contraints for k and ω : (1) $\frac{\hbar\omega - E_F}{\hbar v_F} > k$,(2) $\frac{\omega}{2v_F} - \frac{q}{2} \leq k \leq \frac{\omega}{2v_F} + \frac{q}{2}$ and (3) $\omega > v_F q$. The value of $\frac{\hbar\omega - E_F}{\hbar v_F}$ can be either $\frac{\hbar\omega - E_F}{\hbar v_F} > \frac{\omega}{2v_F} + \frac{q}{2}$ or $\frac{\omega}{2v_F} - \frac{q}{2} \leq \frac{\hbar\omega - E_F}{\hbar v_F} \leq \frac{\omega}{2v_F} + \frac{q}{2}$. We define function

$$f(x) = x\sqrt{1-x^2} + \arcsin x \quad . \tag{2.49}$$

Based on these possibilities, we obtain

$$\begin{aligned}
\mathrm{Im}\,\Pi_{0g}^{\mathrm{inter}}(q,\omega) = &-\frac{1}{\pi\hbar}\frac{\theta(\omega - v_F q)}{v_F\sqrt{\omega^2 - v_F^2 q^2}}\Bigg\{ \int_{\frac{\omega}{2v_F} - \frac{q}{2}}^{\frac{\omega}{2v_F} + \frac{q}{2}} dk \sqrt{v_F^2 q^2 - (\omega + 2kv_F)^2} \\
&\times \theta\left(\frac{\hbar\omega - \hbar v_F q}{2} - E_F\right) + \int_{\frac{\omega}{2v_F} - \frac{q}{2}}^{\frac{\hbar\omega - E_F}{\hbar v_F}} dk \sqrt{v_F^2 q^2 - (\omega + 2kv_F)^2} \\
&\times \theta\left(E_F - \frac{\hbar\omega - \hbar v_F q}{2}\right)\theta\left(\frac{\hbar\omega + \hbar v_F q}{2} - E_F\right)\Bigg\} \\
= &-\frac{q^2}{4\pi\hbar}\frac{\theta(\omega - v_F q)}{\sqrt{\omega^2 - v_F^2 q^2}}\Bigg\{ (f(1) - f(-1))\,\theta\left(\frac{\hbar\omega - \hbar v_F q}{2} - E_F\right) \\
&+ \left(f(1) - f(\frac{2E_F - \hbar\omega}{\hbar v_F q})\right)\theta\left(E_F - \frac{\hbar\omega - \hbar v_F q}{2}\right) \\
&\times \theta\left(\frac{\hbar\omega + \hbar v_F q}{2} - E_F\right)\Bigg\} \quad .
\end{aligned} \tag{2.50}$$

For intraband transition, the constraints are : (1) $\frac{q}{2} - \frac{\omega}{2v_F} \leq k \leq \infty$,(2) $0 \leq k \leq \frac{E_F}{\hbar v_F}$,(3) $k \geq \frac{E_F}{\hbar v_F} - \frac{\omega}{v_F}$and (4) $v_F q > \omega$. The value of $\frac{E_F}{\hbar v_F} - \frac{\omega}{v_F}$ can be positive or negative. For positive value, $\frac{E_F}{\hbar v_F} - \frac{\omega}{v_F} < \frac{q}{2} - \frac{\omega}{2v_F}$ or $\frac{q}{2} - \frac{\omega}{2v_F} \leq \frac{E_F}{\hbar v_F} - \frac{\omega}{v_F} \leq \frac{E_F}{\hbar v_F}$. We define function

$$g(x) = x\sqrt{x^2 - 1} - \ln(x + \sqrt{x^2 - 1}) \quad . \tag{2.51}$$

$$
\begin{aligned}
\mathrm{Im}\,\Pi_{0g}^{\mathrm{intra}}(q,\omega) = &-\frac{1}{\pi\hbar}\frac{\theta(v_{\mathrm{F}}q-\omega)}{v_{\mathrm{F}}\sqrt{v_{\mathrm{F}}^2q^2-\omega^2}}\Bigg\{\int_{\frac{q}{2}-\frac{\omega}{2v_{\mathrm{F}}}}^{\frac{E_{\mathrm{F}}}{\hbar v_{\mathrm{F}}}-\frac{\omega}{v_{\mathrm{F}}}} dk\sqrt{(\omega+2kv_{\mathrm{F}})^2-v_{\mathrm{F}}^2q^2}\\
&\times\theta(\hbar\omega-E_{\mathrm{F}})\theta\left(E_{\mathrm{F}}-\frac{\hbar v_{\mathrm{F}}q-\hbar\omega}{2}\right)+\int_{\frac{q}{2}-\frac{\omega}{2v_{\mathrm{F}}}}^{\frac{E_{\mathrm{F}}}{\hbar v_{\mathrm{F}}}} dk\sqrt{(\omega+2kv_{\mathrm{F}})^2-v_{\mathrm{F}}^2q^2}\\
&\times\theta(E_{\mathrm{F}}-\hbar\omega)\theta\left(E_{\mathrm{F}}-\frac{\hbar v_{\mathrm{F}}q-\hbar\omega}{2}\right)\theta\left(\frac{\hbar v_{\mathrm{F}}q+\hbar\omega}{2}-E_{\mathrm{F}}\right)\\
&+\int_{\frac{E_{\mathrm{F}}}{\hbar v_{\mathrm{F}}}-\frac{\omega}{v_{\mathrm{F}}}}^{\frac{E_{\mathrm{F}}}{\hbar v_{\mathrm{F}}}} dk\sqrt{(\omega+2kv_{\mathrm{F}})^2-v_{\mathrm{F}}^2q^2}\theta(E_{\mathrm{F}}-\hbar\omega)\\
&\times\theta\left(E_{\mathrm{F}}-\frac{\hbar v_{\mathrm{F}}q+\hbar\omega}{2}\right)\Bigg\}\\
=&-\frac{q^2}{4\pi\hbar}\frac{\theta(v_{\mathrm{F}}q-\omega)}{\sqrt{v_{\mathrm{F}}^2q^2-\omega^2}}\Bigg\{\left(g\left(\frac{\hbar\omega+2E_{\mathrm{F}}}{\hbar v_{\mathrm{F}}q}\right)-g(1)\right)\theta(\hbar\omega-E_{\mathrm{F}})\\
&\times\theta\left(E_{\mathrm{F}}-\frac{\hbar v_{\mathrm{F}}q-\hbar\omega}{2}\right)+\left(g\left(\frac{\hbar\omega+2E_{\mathrm{F}}}{\hbar v_{\mathrm{F}}q}\right)-g(1)\right)\theta(E_{\mathrm{F}}-\hbar\omega)\\
&\times\theta\left(E_{\mathrm{F}}-\frac{\hbar v_{\mathrm{F}}q-\hbar\omega}{2}\right)\theta\left(\frac{\hbar v_{\mathrm{F}}q+\hbar\omega}{2}-E_{\mathrm{F}}\right)\\
&+\left(g\left(\frac{\hbar\omega+2E_{\mathrm{F}}}{\hbar v_{\mathrm{F}}q}\right)-g\left(\frac{2E_{\mathrm{F}}-\hbar\omega}{\hbar v_{\mathrm{F}}q}\right)\right)\theta(E_{\mathrm{F}}-\hbar\omega)\\
&\times\theta\left(E_{\mathrm{F}}-\frac{\hbar v_{\mathrm{F}}q+\hbar\omega}{2}\right)\Bigg\}\quad. \qquad (2.52)
\end{aligned}
$$

The real part of polarization is expressed in Eq. (2.53). The summation over k is changed into integration on ϕ and k. We do not split the real part of polarization into interband and intraband, but it is split only by index α.

Fig. 2.7: Fig/fig2k5.eps

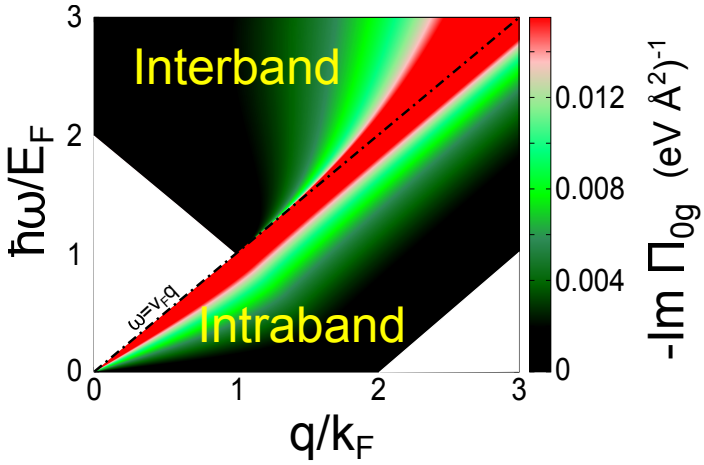

Figure 2.5 The imaginary part of doped graphene polarization. Both of interband and intraband polarization are shown within one figure. The boundary between them is $\omega = v_{\mathrm{F}} q$.

$$\begin{aligned}
\mathrm{Re}\,\Pi_{0g}(q,\omega) =& \frac{2}{A}\sum_{k,\alpha,\beta}\frac{n_{\alpha,k}-n_{\alpha\beta,k+q}}{\hbar\omega+\alpha(\hbar v_{\mathrm{F}}k-\hbar v_{\mathrm{F}}\beta|\mathbf{k}+\mathbf{q}|)}\left(1+\frac{k+q\cos\phi}{|\mathbf{k}+\mathbf{q}|}\right)\\
=& \frac{1}{2\pi^2\hbar v_{\mathrm{F}}}\sum_{\alpha}\int dk\theta(k-\frac{E_{\mathrm{F}}}{\hbar v_{\mathrm{F}}})\\
&\times\int_0^{2\pi}d\phi\left(1+\frac{v_{\mathrm{F}}^2q^2-(2v_{\mathrm{F}}k+\alpha\omega)^2}{\omega^2-v_{\mathrm{F}}^2q^2+2kv_{\mathrm{F}}\omega\alpha-2kv_{\mathrm{F}}^2q\cos\phi}\right) \quad . \qquad (2.53)
\end{aligned}$$

The integration on ϕ is done within complex plane and depends on α. For $\alpha = 1$ and $\alpha = -1$, the integration becomes as below, respectively, (For $\alpha = 1$)

$$\begin{aligned}
\mathrm{Re}\,\Pi^{+}_{0g}(q,\omega) =& \frac{1}{2\pi^2\hbar v_{\mathrm{F}}}\int dk\theta(k-\frac{E_{\mathrm{F}}}{\hbar v_{\mathrm{F}}})\\
&\times\int_0^{2\pi}d\phi\left(1+\frac{v_{\mathrm{F}}^2q^2-(2v_{\mathrm{F}}k+\omega)^2}{\omega^2-v_{\mathrm{F}}^2q^2+2kv_{\mathrm{F}}\omega-2kv_{\mathrm{F}}^2q\cos\phi}\right)\\
=& \frac{1}{2\pi^2\hbar v_{\mathrm{F}}}\int dk\theta(k-\frac{E_{\mathrm{F}}}{\hbar v_{\mathrm{F}}})\left(2\pi+2\pi\left(v_{\mathrm{F}}^2q^2-(2v_{\mathrm{F}}k+\omega)^2\right)\right)\\
&\times\frac{\left(\theta(\omega-v_{\mathrm{F}}q)-\theta(v_{\mathrm{F}}q-\omega)\theta\left(\frac{q-\frac{\omega}{v_{\mathrm{F}}}}{2}-k\right)\right)}{\sqrt{(\omega^2-v_{\mathrm{F}}^2q^2+2kv_{\mathrm{F}}\omega)^2-4k^2v_{\mathrm{F}}^4q^2}} \qquad (2.54)
\end{aligned}$$

(For α = -1)

$$\begin{aligned}
\mathrm{Re}\,\Pi_{0g}^{-}(q,\omega) =& \frac{1}{2\pi^2\hbar v_\mathrm{F}}\int dk\theta(k-\frac{E_\mathrm{F}}{\hbar v_\mathrm{F}}) \\
&\times\int_0^{2\pi} d\phi\left(1+\frac{v_\mathrm{F}^2q^2-(2v_\mathrm{F}k-\omega)^2}{\omega^2-v_\mathrm{F}^2q^2-2kv_\mathrm{F}\omega-2kv_\mathrm{F}^2q\cos\phi}\right) \\
=& \frac{1}{2\pi^2\hbar v_\mathrm{F}}\int dk\theta(k-\frac{E_\mathrm{F}}{\hbar v_\mathrm{F}})\left(2\pi+2\pi\left(v_\mathrm{F}^2q^2-(2v_\mathrm{F}k-\omega)^2\right)\right) \\
&\times\left(\theta(\omega-v_\mathrm{F}q)\theta\left(\frac{\frac{\omega}{v_\mathrm{F}}-q}{2}-k\right)-\theta(\omega-v_\mathrm{F}q)\theta\left(k-\frac{\frac{\omega}{v_\mathrm{F}}+q}{2}\right)\right. \\
&\left.\times\,\theta(v_\mathrm{F}q-\omega)\theta\left(\frac{\frac{\omega}{v_\mathrm{F}}+q}{2}-k\right)\right) \\
&\times\frac{1}{\sqrt{(\omega^2-v_\mathrm{F}^2q^2-2kv_\mathrm{F}\omega)^2-4k^2v_\mathrm{F}^4q^2}} \quad . \qquad (2.55)
\end{aligned}$$

The total real part of polarization is the sum of $\mathrm{Re}\,\Pi_{0g}(q,\omega) = \mathrm{Re}\,\Pi_{0g}^{+}(q,\omega) + \mathrm{Re}\,\Pi_{0g}^{-}(q,\omega)$. Here, we give the final result of integration for real part of polarization.

$$\begin{aligned}
\mathrm{Re}\,\Pi_{0g}(q,\omega) =& -\frac{2}{\pi\hbar v_\mathrm{F}}\frac{E_\mathrm{F}}{\hbar v_\mathrm{F}}+\frac{q^2}{4\pi\hbar}\frac{\theta(\omega-v_\mathrm{F}q)}{\sqrt{\omega^2-v_\mathrm{F}^2q^2}}\left\{g\left(\frac{\hbar\omega+2E_\mathrm{F}}{\hbar v_\mathrm{F}q}\right)\right. \\
&-\theta\left(\frac{\frac{\omega}{v_\mathrm{F}}-q}{2}-\frac{E_\mathrm{F}}{\hbar v_\mathrm{F}}\right)g\left(\frac{\hbar\omega-2E_\mathrm{F}}{\hbar v_\mathrm{F}q}\right) \\
&\left.+\,\theta\left(\frac{E_\mathrm{F}}{\hbar v_\mathrm{F}}-\frac{\frac{\omega}{v_\mathrm{F}}+q}{2}\right)g\left(\frac{2E_\mathrm{F}-\hbar\omega}{\hbar v_\mathrm{F}q}\right)\right\} \\
&-\frac{q^2}{4\pi\hbar}\frac{\theta(v_\mathrm{F}q-\omega)}{\sqrt{v_\mathrm{F}^2q^2-\omega^2}}\left[\theta\left(\frac{\frac{\omega}{v_\mathrm{F}}+q}{2}-\frac{E_\mathrm{F}}{\hbar v_\mathrm{F}}\right)\right. \\
&\times\left\{f(1)-f\left(\frac{2E_\mathrm{F}-\hbar\omega}{\hbar v_\mathrm{F}q}\right)\right\}+\theta\left(\frac{q-\frac{\omega}{v_\mathrm{F}}}{2}-\frac{E_\mathrm{F}}{\hbar v_\mathrm{F}}\right) \\
&\left.\times\left(f(1)-f\left\{\frac{\hbar\omega+2E_\mathrm{F}}{\hbar v_\mathrm{F}q}\right)\right\}\right] \quad . \qquad (2.56)
\end{aligned}$$

The function $f(x)$ and $g(x)$ have been defined in Eqs. (2.49), and (2.51). The total of polarization function is $\Pi_{0g}(q,\omega) = \mathrm{Re}\,\Pi_{0g}(q,\omega) + \mathrm{Im}\,\Pi_{0g}(q,\omega)$. Thus, the dielectric function of doped graphene can be calculated using Eq. (2.44), with doped polarization function of graphene Eqs. (2.50), and (2.52),(2.56). The plot of real part of dielectric function for doped graphene is presented in Fig.. 2.6. At certain frequency, the real part of dielectric function is zero. This zero value of dielectric function is related to plasmon, which will be discussed in the next chapter.

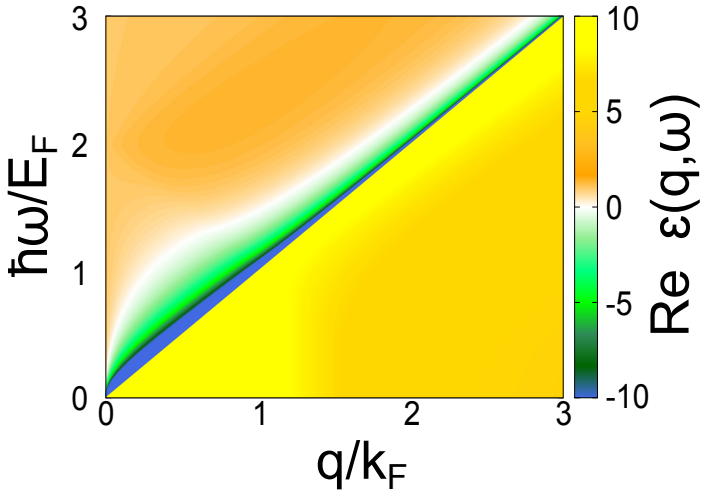

Figure 2.6 The real part of doped graphene dielectric function.

The imaginary part of doped graphene dielectric function is plotted as below.

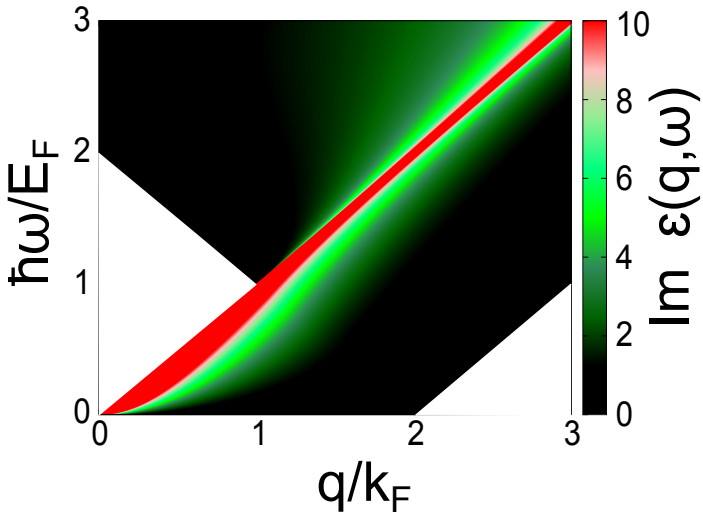

Figure 2.7 The imaginary part of doped graphene dielectric function.

Fig. 2.6: Fig/fig2k6.eps
Fig. 2.7: Fig/fig2k7.eps

Chapter 3

Graphene Surface Plasmon Properties

In this chapter, the graphene surface plasmon (SP) properties are explained. The discussed properties in this chapter are the dispersion relation of surface plasmon and the damping. SP propagates at certain frequency ω and wave vector q, which are determined by the dispersion relation. The dispersion relation relates the frequency of SP to its wave vector. The dispersion relation can be obtained from dielectric function as is discussed in chapter 2. SP, at certain frequency and wave vector, experiences damping. This damping is related to imaginary part of the polarization function, which governs the energy dissipation of SP wave [24, 23]. SP acquire finite life time, when it is damped out.

3.1 Graphene surface plasmon dispersion

Graphene surface plasmon (SP) dispersion relation relates the frequency of SP to its wave vector. The dispersion relation can be obtained from the dielectric function. The zeroes of dielectric function determines the dispersion relation of SP. From Eq. (2.19), we have $\varphi_{\text{ext}}(q,\omega) = \varepsilon(q,\omega)\varphi(q,\omega)$, where $\varphi(q,\omega)$ is total potential inside the system. If the dielectric function $\varepsilon(q,\omega) = 0$, we can have total potential inside system even though we do not have external potential exerted to system. To sustain this total potential, oscillation of charge is required. That is the reason, we can have SP if the dielectric function is zero.

From Eq. (2.44) , dielectric function can be written as

$$\epsilon(q,\omega) = 1 - \frac{e^2}{2\varepsilon_0 q}\Pi_{0g}(q,\omega) \quad . \tag{3.1}$$

Since the polarization function is a complex function, the dielectric function is also a complex function. Thus, to find the zeroes of dielectric function is not easy because of this complex function. The zeroes of Eq. (3.1) should satisfy $1 = \frac{e^2}{2\varepsilon_0 q}\Pi_{0g}(q, \Omega - i\gamma)$, where SP can occur at $\omega = \Omega - i\gamma$ and γ is the damping constant. However, if we consider that damping γ is sufficiently small ($\gamma \ll \Omega$), the real and imaginary part of ω can be separated [25].

$$1 = \frac{e^2}{2\varepsilon_0 q}\mathrm{Re}\,\Pi_{0g}(q,\Omega) \tag{3.2}$$

$$\gamma = \mathrm{Im}\,\Pi_{0g}(q,\Omega)\left[\frac{\partial \mathrm{Re}\,\Pi_{0g}(q,\omega)}{\partial\omega}\right]^{-1}_{\Omega} \tag{3.3}$$

The dispersion relation is determined by Eq. (3.2). The SP occurs at frequency Ω. In this case, only real part of polarization is needed to find the dispersion relation, or equivalently, zero value of the real part of the dielectric function determines the dispersion relation. The damping constant γ is determined by Eq. (3.3). Hereafter, we consider undoped and doped graphene.

First, the case of undoped graphene is discussed. The real part of polarization function can be obtained from Eq. (2.43). From Eq. (3.2), we get

$$1 = -\frac{e^2}{2\varepsilon_0 q}\left(\frac{q^2}{4\hbar}\frac{\theta(v_\mathrm{F} q - \Omega)}{\sqrt{v_\mathrm{F}^2 q^2 - \Omega^2}}\right) \quad . \tag{3.4}$$

Eq. (3.4) gives no solution for Ω, because the left-hand side is positive, while the right-hand side gives a negative value. It can be concluded that for undoped graphene, SP cannot exist. This can be understood by following explanation : for undoped case, there is no free charge carrier, so we have no possibilities of charge oscillation.

For doped case, we use real part of polarization from Eq. (2.56) and plug it into Eq. (3.2). The solution is plotted in Fig. 3.1. From Eq. (3.2), we can also say that zero of real part of dielectric function determines the SP dispersion. It can be seen in Fig. 2.6 as white line. Then, it is concluded that SP exists in case of doped graphene.

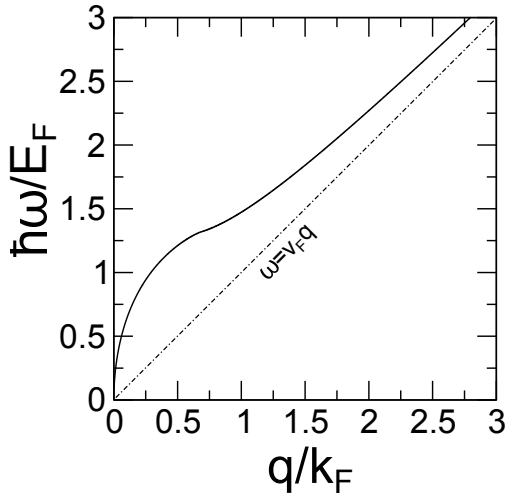

Figure 3.1 SP dispersion for doped graphene. The dash line is the electronic energy dispersion $\omega = v_{\mathrm{F}} q$.

Fig. 3.1 shows that the SP dispersion relation of doped graphene in the air, which is the solution of Eq. (3.2). The frequency is normalized to E_{F}, while the wave vector is normalized to Fermi wave vector k_F. Thus, the shape of dispersion relation remains the same, even though the E_{F} is changed. For small q ($q \ll k_F$), the dispersion is a function of $\sqrt{q}$. This $\sqrt{q}$ dependence of frequency is the same as SP of normal 2D electron gas, which also has the $\sqrt{q}$ dependence of frequency at small wave vector. The dispersion of graphene SP at small wave vector can be derived as if we expand the real part of polarization at small q as follows.

From Fig. 3.1, we know that SP occurs at $\omega > v_{\mathrm{F}} q$. The real part of polarization function (Eq.(2.56)) at $\omega > v_{\mathrm{F}} q$ can be written as

$$\mathrm{Re}\,\Pi_{0g}(q,\omega) = -\frac{2}{\pi\hbar v_{\mathrm{F}}}\frac{E_{\mathrm{F}}}{\hbar v_{\mathrm{F}}} + \frac{q^2}{4\pi\hbar}\frac{1}{\sqrt{\omega^2 - v_{\mathrm{F}}^2 q^2}}\left(g\left(\frac{\hbar\omega + 2E_{\mathrm{F}}}{\hbar v_{\mathrm{F}} q}\right) - g\left(\frac{2E_{\mathrm{F}} - \hbar\omega}{\hbar v_{\mathrm{F}} q}\right)\right), \tag{3.5}$$

Here $g(x)$ is given in Eq (2.51). For $q \ll k_{\mathrm{F}}$, the x of $g(x)$ is large, so it can be approximated as $g(x) \approx x^2 - \ln 2x$. We will have

Fig. 3.1: Fig/fig3k1.eps

$$-g\left(\frac{\hbar\omega+2E_{\mathrm{F}}}{\hbar v_{\mathrm{F}}q}\right)-g\left(\frac{2E_{\mathrm{F}}-\hbar\omega}{\hbar v_{\mathrm{F}}q}\right)=\left(\frac{\hbar\omega+2E_{\mathrm{F}}}{\hbar v_{\mathrm{F}}q}\right)^2-\left(\frac{2E_{\mathrm{F}}-\hbar\omega}{\hbar v_{\mathrm{F}}q}\right)^2+\ln\frac{2E_{\mathrm{F}}-\hbar\omega}{\hbar\omega+2E_{\mathrm{F}}}$$
$$\approx\frac{8E_{\mathrm{F}}\omega}{\hbar v_{\mathrm{F}}^2q^2} \quad , \tag{3.6}$$

where we neglect the logarithmic term for simplicity. Since for small q, $\frac{1}{\sqrt{\omega^2-v_{\mathrm{F}}^2q^2}}\approx\frac{1}{\omega}\left(1+\frac{v_{\mathrm{F}}^2q^2}{2\omega^2}\right)$, the real part of polarization function at small q is given by.

$$\mathrm{Re}\,\Pi_{0g}(q,\omega)=-\frac{2}{\pi\hbar v_{\mathrm{F}}}\frac{E_{\mathrm{F}}}{\hbar v_{\mathrm{F}}}+\frac{q^2}{4\pi\hbar\omega}\left(1+\frac{v_{\mathrm{F}}^2q^2}{2\omega^2}\right)\left(\frac{8E_{\mathrm{F}}\omega}{\hbar v_{\mathrm{F}}^2q^2}\right)$$
$$=\frac{E_{\mathrm{F}}}{\pi}\left(\frac{q}{\hbar\omega}\right)^2 \quad . \tag{3.7}$$

putting Eq. (3.7) to Eq. (3.2), we will have frequency Ω as function of wave vector which is $\sqrt{q}$ dependent.

$$\Omega(q)=\frac{1}{\hbar}\sqrt{\frac{e^2E_{\mathrm{F}}q}{2\pi\varepsilon_0}} \tag{3.8}$$

For large q ($q>k_F$), the dispersion becomes linear to q as shown in Fig. 3.1. The dispersion seems to be almost parallel to electron dispersion ($\omega=v_{\mathrm{F}}q$) for large q.

3.2 Graphene surface plasmon damping

Now we discuss the damping of SP. This damping is related to imaginary part of polarization, which governs the energy dissipation [24, 23]. SP acquires finite life time, when it is damped out. The damping of SP can be visualized by imaginary part of polarization function. The higher the value of imaginary part of polarization, the higher the damping felt by SP.

Fig. 3.2(a) shows the SP dispersion (blue line) together with the plot of imaginary part of polarization ($\mathrm{Im}\,\Pi_{0g}(q,\omega)$) (coloured plot). The $\mathrm{Im}\,\Pi_{0g}(q,\omega)$ is associated with the ability of SP wave to dissipate energy [24]. This gives damping to SP. The dissipated energy from SP wave is absorbed by an electron. The electron will be excited to form electron-hole pair (single - particle excitation). An electron is excited to a state outside the Fermi sea. The possible range of q and ω for single - particle

Fig. 3.2: Fig/fig3k2.eps

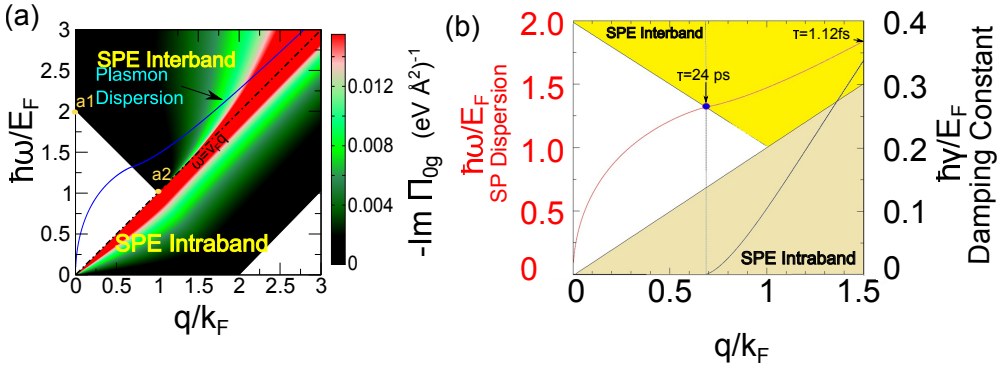

Figure 3.2 (a) SP dispersion (blue line) of doped graphene plotted together with plot of imaginary part of polarization function (coloured plot). (b) SP dispersion (red line) plotted together with damping constant (black line).

excitation is given by the coloured region in Fig.. 3.2(a). Hence, the SP within this region is damped out because of electron-hole pair excitation and acquires a finite life time.

The excitation of electron can be either interband or intraband, which are shown in Fig.. 3.2(a) as single particle excitation (SPE) region of interband and intraband transition. The electron can undergo interband transition and form an electron-hole pair. The value of $\mathrm{Im}\,\Pi_{0g}(q,\omega)$ reflects the probability of excitation. The SP dispersion couples with only the SPE interband excitation as shown in Fig. 3.2(a). At the SPE region, SP can survive even though it is damped out. It can be seen, that the higher the SP frequency Ω (or equivalently q), the higher the value of $\mathrm{Im}\,\Pi_{0g}(q,\Omega)$ (red color). Therefore high frequency SP experience high damping and we can expect small life time for high frequency SP, because of high damping.

The excitation of electron cannot occur within white region of Fig. 3.2(a). This is because there is no final states available for excitation as shown in Fig. 3.3(a). In this region, electron cannot absorb energy from SP wave, therefore SP is not damped and long live. The point a1 in Fig. 3.2 is the first direct transition of electron, where the transfer momentum of electron (q) is $q = 0$ (see Fig. 3.3(a). Therefore, we need excitation energy to be $2E_{\mathrm{F}}$. Direct transition can occur only for interband transition. From Fig. 3.2(a), we see that the value of $\mathrm{Im}\,\Pi_{0g}(0,\omega)$ is small, that means the probability

Fig. 3.3: Fig/fig3k3.eps

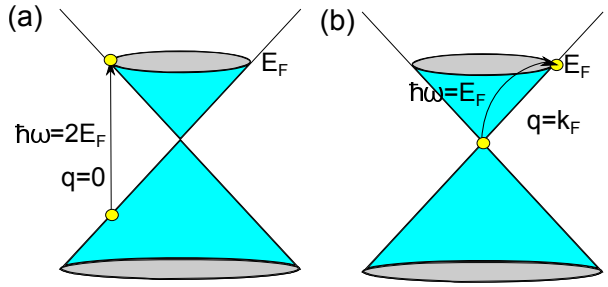

Figure 3.3 (a) The transition for point a1 of Fig. 3.2(a), which is the first direct transition of electron. The required excitation energy is $2E_{\rm F}$ for the first direct transition of electron $q = 0$. (b) The transition for point a2 of Fig. 3.2(a), which is the lowest excitation energy for interband transition of electron. The required energy is $E_{\rm F}$ and $q = k_F$.

to have this excitation is small. The point a2 in Fig. 3.2 is the lowest excitation energy to have interband transition as shown in Fig. 3.3(b). Electron undergoes transition from Dirac point to state just above Fermi energy.

The damping can be quantified by damping constant, which is related to SP life time. Damping constant γ can be calculated from Eq. (3.3). Fig. 3.2(b) shows γ as a function of SP wave vector (q). We see that γ increases as function of q from $q/k_{\rm F} \sim 0.87$. This is related to previous discussion on imaginary part of polarization. When SP frequency Ω (or equivalently q) gets higher, the value of $\mathrm{Im}\,\Pi_{0g}(q, \Omega)$ also increases, this in turns increases the damping. The life time of SP (τ) is determined by the damping constant. The life time of SP is written as [47]

$$\tau(q) = \frac{1}{2\gamma(q)} \quad . \tag{3.9}$$

As SP enters the SPE interband, it immediately acquires a finite life time. From Fig. 3.2(b), we see that the point of entrance is approximately at $q = 0.68k_F$. At that point, for a fixed value of $E_{\rm F} = 1$ eV, SP life time is around 24 ps. For $q < 0.68k_{\rm F}$, $\gamma = 0$, therefore the life time is infinity (not damped). As q increases, the life time decreases fast. For instance, at $q = 1.5k_F$, τ is only 1.12 fs. The τ dependency on q is shown in Fig. 3.4 .

The origin of the SP damping is known as Landau's damping in plasma physics [7, 24, 25]. We do not discuss it in deep in this thesis, but we will give a simple classical

Fig. 3.4: Fig/fig3k4.eps

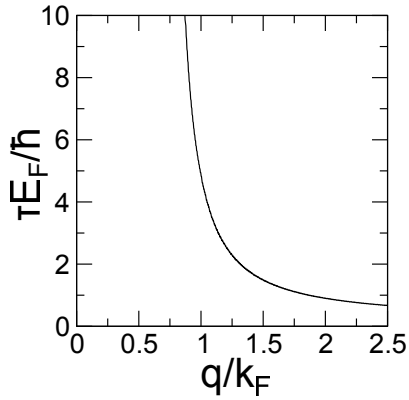

Figure 3.4 SP life time (τ) is plotted as a function of SP wave vector q.

picture of it. Landau's damping occurs at classical plasma wave. This damping reduces the energy of plasma wave. This damping is due to different velocities of resonance electrons. A resonance electron is defined by the electron whose velocity is almost the same as the plasma wave velocity. The velocity of resonance electron can be slightly higher or slightly lower than the wave velocity. The slightly faster electrons will give their energy to wave, we can picture it in our mind that these faster electrons "push" the wave and give their energy to wave. The slightly slower electrons will absorb energy from the wave, they are like being pushed by the wave. Because of classical Boltzmann distribution for electrons, there are more slightly slower electrons than slightly faster ones. Therefore, there are more energy absorption by electrons. This differences between absorption and emission energy reduce the plasma wave energy and gives damping to plasma wave. This absorbed energy is used by electrons for electron-hole excitation.

Chapter 4

Tunable Electromagnetic Wave Absorption by Graphene and Surface Plasmon Excitation

In this chapter, we will investigate the ability of graphene to absorb the incoming electromagnetic (EM) wave. First we begin by formulating the absorption, reflectance and transmittace probabilities of the EM wave by graphene in between two dielectric media. We use the conductivity of graphene that can be obtained from dielectric function of graphene in chapter2. We will see, provided that we have certain geometry and certain range of frequency, we can have very high absorption of EM wave. This high absorption probability can also be tuned by E_{F}. We argue that this high absorption probability will be related to excitation of SP.

4.1 EM wave absorption by graphene wrapped by 2 dielectric media

Let us discuss the formulation of absorption, reflectance and transmittance of EM wave penetrating to graphene. The easiest way to obtain them is to solve them by solving the Maxwell equations for EM wave with boundary conditions. We consider that graphene is placed between two dielectric media as shown in Fig. 4.1.

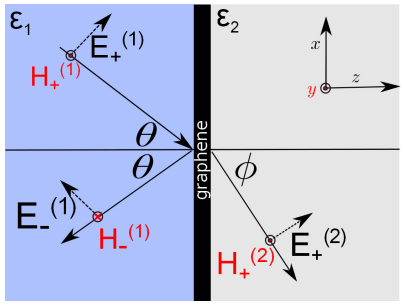

Figure 4.1 Graphene is placed between two dielectric media with dielectric constants ε_1 and ε_2. Graphene thickness is exaggerated. The incident EM wave comes at an angle θ in medium 1 (left) and is refracted at an angle ϕ in medium 2 (right). The EM wave is p-polarized.

Graphene is modeled as a conducting interface with the conductivity σ between two dielectric media with dielectric constants ε_1 and ε_2. The absorption, reflectance and transmittance probabilities for this geometry can be calculated by utilizing the boundary conditions from the Maxwell's equations. If we adopt the p-polarization of EM wave as shown in Fig. 4.1, we can obtain two boundary conditions for the electric field $E^{(i)}$ and magnetic field $H^{(i)}$ $(i = 1, 2)$ as follows:

$$E_+^{(1)} \cos\theta + E_-^{(1)} \cos\theta = E_+^{(2)} \cos\phi, \tag{4.1}$$

$$H_+^{(2)} - (H_+^{(1)} - H_-^{(1)}) = -\sigma E_+^{(2)} \cos\phi, \tag{4.2}$$

where $+(-)$ index denotes the right-(left-)going waves according to Fig. 4.1, θ is the incident and reflection angle, ϕ is the refraction angle, and σ is the conductivity of graphene. [49]. Eq. (4.1) and (4.2) come from Faraday law and Ampere law, respectively. The E and H fields are also related each other in terms of the EM wave impedance in units of Ohm for each medium:

$$Z_i = \frac{E_i}{H_i} = \frac{377}{\sqrt{\varepsilon_i}} \text{ Ohm}, \quad (i = 1, 2), \tag{4.3}$$

where the constant 377 Ohm is the impedance of vacuum $Z_0 = \sqrt{\mu_0/\varepsilon_0}$, μ_0 and ε_0 are vacuum magnetic susceptibility and permitvity, respectively. Quantities ϕ, θ, and Z_i are related by Snell's law $Z_2 \sin\theta = Z_1 \sin\phi$. Solving Eqs. (4.1)-(4.3), we obtain the reflectance R, transmittance T, and absorption probabilities A of the EM wave as

Fig. 4.1: Fig/fig4k1.eps

follows:

$$\begin{aligned} R &= \left| \frac{E_1^{(-)}}{E_1^{(+)}} \right|^2 \\ &= \left| \frac{Z_2 \cos\phi - Z_1 \cos\theta - Z_1 Z_2 \sigma \cos\theta \cos\phi}{Z_2 \cos\phi + Z_1 \cos\theta + Z_1 Z_2 \sigma \cos\theta \cos\phi} \right|^2, \\ T &= \frac{\cos\phi}{\cos\theta} \frac{Z_1}{Z_2} \left| \frac{E_2^{(+)}}{E_1^{(+)}} \right|^2 \\ &= \frac{4 Z_1 Z_2 \cos\theta \cos\phi}{\left| Z_2 \cos\phi + Z_1 \cos\theta + Z_1 Z_2 \sigma \cos\theta \cos\phi \right|^2}, \\ A &= 1 - R - T, \end{aligned} \tag{4.4}$$

where the values of R, T, and A can be denoted in terms of percentage $(0 - 100\%)$. Note that the factor Z_1/Z_2 in T of Eq. (4.4) comes from the different velocities of the EM wave in medium 1 and medium 2.

The EM wave absorption A is determined by the conductivity σ which describes the electron transition caused by the optical absorption. Here we show an alternative way to derive σ. σ of graphene is derived from the dielectric function ε using a random-phase approximation (RPA). Since the coupling between the EM wave and matter occurs only at long wavelength, we focus our calculation only at $q \to 0$ case. The real part of polarization at $q \to 0$ can be obtained from Eq. (3.5) and the imaginary part of polarization at $q \to 0$ can be obtained from Eq. (2.50). Plugging the polarization function to Eq. (3.1), the RPA dielectric function of graphene as a function of wavevector q and angular frequency ω of the EM wave for a given Fermi energy E_F is expressed by [26]

$$\begin{aligned} \varepsilon(q \to 0, \omega) =& 1 - \left(\frac{e^2}{2\varepsilon_0 q} \right) \frac{q^2}{2\pi\hbar\omega} \times \left[\frac{2E_\mathrm{F}}{\hbar\omega} \right. \\ & \left. + \frac{1}{2} \ln \left| \frac{2E_\mathrm{F} - \hbar\omega}{2E_\mathrm{F} + \hbar\omega} \right| - i\frac{\pi}{2} \Theta(\hbar\omega - 2E_\mathrm{F}) \right], \end{aligned} \tag{4.5}$$

where e is the fundamental electron charge and Θ is the Heaviside step function. The relation between σ and ε can be obtained from the continuity equation,

$$\nabla \cdot \mathbf{J} + e\frac{\partial \rho}{\partial t} = 0 \tag{4.6}$$

$$-ie\omega\rho(q,\omega) + i\mathbf{q} \cdot \mathbf{J} = 0 \quad , \tag{4.7}$$

where $\mathbf{J} = \sigma(q,\omega)\mathbf{E}(q,\omega) = -i\sigma(q,\omega)\mathbf{q}\varphi_{\rm ext}(q,\omega)$. Eq. (4.7) is obtained by Fourrier transform of Eq. (4.6). Putting Eq. (2.22), we get the following equation

$$\sigma(q,\omega) = \frac{ie^2\omega}{q^2}\Pi(q,\omega) \quad . \tag{4.8}$$

Since we want to relate ε and σ, by using Eq. 2.24, Eq. 4.8 can be rewritten as

$$\varepsilon(q,\omega) = \frac{1}{1-\frac{iv(q)\sigma(q,\omega)q^2}{e^2\omega}} \tag{4.9}$$

$$\approx 1 + \frac{iv(q)\sigma(q,\omega)q^2}{e^2\omega} \quad . \tag{4.10}$$

Eq. (4.10) is valid for small q. In term of ε, σ is expressed as

$$\sigma\left(q,\omega\right) = \frac{i2\varepsilon_0\omega}{q}\left(1-\varepsilon\left(q,\omega\right)\right), \tag{4.11}$$

obtained in (q,ω) space. [54]. Here we use $v(q) = e^2/2\varepsilon_0 q$. Plugging Eq. (4.5) to Eq. (4.11), σ can be written as [55]

$$\begin{aligned}\sigma\left(\omega\right) \equiv& \sigma_D + \text{Re }\sigma_E + \text{Im }\sigma_E \\ =& \frac{E_{\rm F}e^2}{\pi\hbar}\frac{i}{\hbar\omega+i\Gamma} + \frac{e^2}{4\hbar}\Theta\left(\hbar\omega-2E_{\rm F}\right) \\ &+ \frac{ie^2}{4\pi\hbar}\ln\left|\frac{2E_{\rm F}-\hbar\omega}{2E_{\rm F}+\hbar\omega}\right|.\end{aligned} \tag{4.12}$$

The first term in Eq. (4.12) is the intraband conductivity, which is known as the Drude conductivity σ_D. We add a spectral width Γ as a phenomenological parameter for scattering rate and it depends on $E_{\rm F}$ as $\Gamma = \hbar e v_{\rm F}^2/\mu E_{\rm F}$, [13] where $v_{\rm F} = 10^6$ m/s is the Fermi velocity of graphene, $\mu = 10^4$ cm^2/Vs is the electron mobility. The second and the third terms in Eq. (4.12) correspond to the real part and the imaginary part of interband conductivity σ_E, respectively. By inserting Eq. (4.12) and Eq. (4.3) into Eq. (4.4), we get A, R, T as a function of $E_{\rm F}$ and incidence angle θ. Both σ_D and σ_E affect the EM wave absorption and each contribution as discussed below.

Let us see how the EM wave absorption in graphene can be modified under some certain conditions. Firstly, in Fig. 4.2(a), we reproduce the 2.3% optical absorption if graphene is put in a vacuum, [56] i.e. $\varepsilon_1 = \varepsilon_2 = 1$ with $E_{\rm F} = 0.64$ eV, $\theta = 0°$. The absorption A is associated with the real part of σ as shown by the same shape of both curves in Figs. 4.2(a) and (b). [54] In Fig. 4.2(b), the conductivity of graphene

Fig. 4.2: Fig/fig4k2.eps

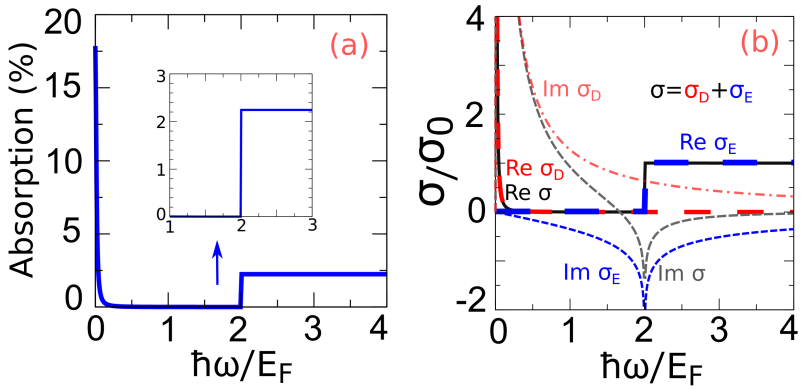

Figure 4.2 (a) The absorption spectra of EM wave at $E_{\rm F} = 0.64$ eV, $\varepsilon_1 = \varepsilon_2 = 1$ and $\theta = 0^\circ$. Inset shows the expanded section of absorption for $1 \leq \hbar\omega/E_{\rm F} \leq 3$. (b) The normalized optical conductivity.

[Eq. (4.12)] normalized by $\sigma_0 = e^2/4\hbar$ is shown. The A value of 2.3% is obtained when $\hbar\omega > 2E_{\rm F}$ [inset of Fig. 4.2(a)] because at this region, the real part of total conductivity σ is a constant σ_0 [see Fig. 4.2(b)] which comes from Re σ_E (while σ_D is negligible). When $\hbar\omega/E_{\rm F} \approx 0$ [Fig. 4.2(a)], it can be seen that the A value becomes large ($\sim 20\%$) due to the Drude conductivity Re σ_D as shown in Fig. 4.2(b). In this case, Re σ_D plays the main role in σ. Because of the large A value in this region, we let the parameter $\hbar\omega = 0.1$ meV (equivalent to $f = 24.2$ GHz or microwave) and $E_{\rm F} = 0.64$ eV such that a large A is expected when the incident angle θ is changed.

We introduce total internal reflection (TIR) geometry for getting high absorption. This is because TIR suppresses the transmittance and thus EM wave can either be reflected or absorbed by graphene. Since TIR increases the probability of absorption, EM wave energy is divided only into two channels (absorption and transmission), not three. In TIR, EM wave comes from medium with higher dielectric constant to medium with lower dielectric constant ($\varepsilon_1 > \varepsilon_2$). When TIR occurs, no EM wave can be transmitted, and thus the EM wave can either be reflected or absorbed by graphene. Here we set $\varepsilon_1 = 2.25$ and $\varepsilon_2 = 1.25$ which corresponds to $\theta_c = 48.19^\circ$. In Fig. 4.3(a), we show A, R and T as a function of θ. As seen in Fig. 4.3(a), $T = 0$ if $\theta \geq \theta_c$. Interestingly, A becomes almost unity at an angle around 85°, hence graphene absorbs all of the incoming EM waves, where $R = 0$. The dip in the A spectrum

Fig. 4.3: Fig/fig4k3.eps

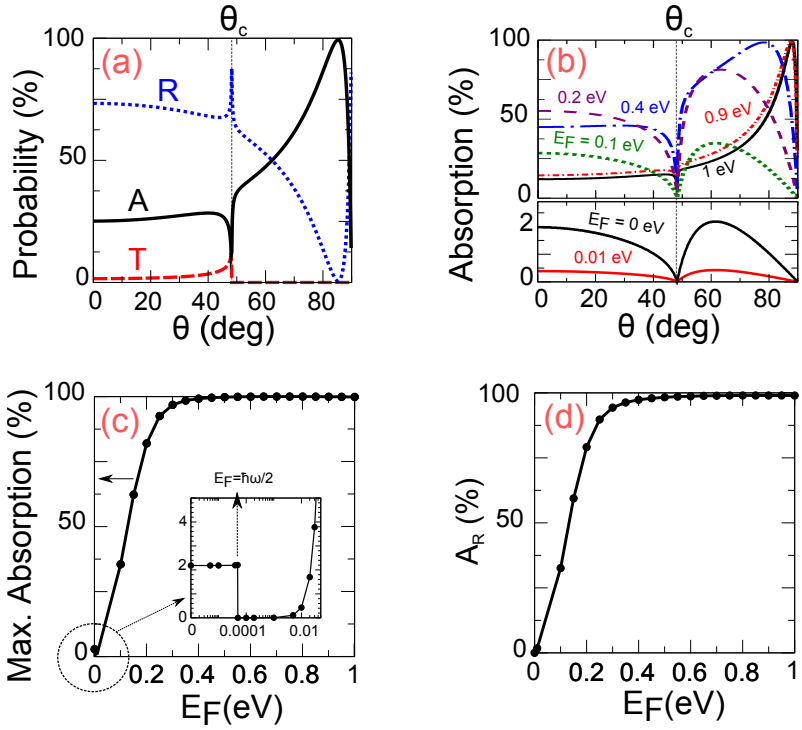

Figure 4.3 (a) Absorption probability (A), reflectance (R) and transmittance (T). The A value of 0 (100%) expresses the zero (perfect) absorption of the EM wave. The graphene ($E_{\rm F} = 0.64$ eV) is sandwiched between two media with $\varepsilon_1 = 2.25$ and $\varepsilon_2 = 1.25$. (b) Absorption for several different $E_{\rm F}$ values. (c) Maximum value of A as a function of $E_{\rm F}$. Inset shows the enlarged region of the maximum A for small $E_{\rm F}$ values. (d) Absorption range (A_R) as a function of $E_{\rm F}$.

(Fig. 4.3(a)) indicates the beginning of TIR, where R reaches the maximum value. In Fig. 4.3(b) we show the $E_{\rm F}$ dependence of A as a function of θ for several $E_{\rm F}$ values. Furthermore, from each absorption peak as obtained in Fig. 4.3(b), we can plot the maximum value of A a function of $E_{\rm F}$ [see Fig. 4.3(c)]. The maximum A value rapidly increases with increasing $E_{\rm F}$ and is saturated near 100% for $E_{\rm F} \geq 0.4$ eV. For $\hbar\omega/2 < E_{\rm F} < 0.01$ eV, A is nearly 0 as we can see in Fig. 4.3(b) and in the inset of Fig. 4.3(c).

It is expected that when $E_{\rm F}$ decreases, A will decrease monotonically to zero. However, this is not the case as we can see in Fig. 4.3(b) and in the inset of Fig. 4.3(c). Even when we set $E_{\rm F}$ equals zero (or $\hbar\omega \geq 2E_{\rm F}$), the A value is around 2.2%. This is due to the vanishing intraband transition, while the interband transition dominates

with the total conductivity σ is governed by the constant σ_0 for $\hbar\omega \geq 2E_F$. Therefore, although the E_F decreases to zero, absorption is not zero. At the same time, for $\hbar\omega < 2E_F$, Drude conductivity dominates and conductivity is proportional to E_F as we can realize from Eq. (4.12). This is the reason why A for $E_F = 0.01$ eV is smaller than that for $E_F = 0$ eV.

In Fig. 4.3(d), we define the absorption range (A_R) as the difference between the maximum$A$ value at $E_F \neq 0$ and at $E_F = 0$ while keeping θ_{max} for $E_F \neq 0$. θ_{max} is the angle which gives the largest A in Fig. 4.3. We can see that A_R starts to stabilize from $E_F = 0.4$ eV at around 99%. It means that if we change the E_F from $E_F > 0.4$ eV to zero, nearly perfect switching of the reflected EM wave can be observed, and this behavior could be useful for some device applications.

4.2 Application of absorption tunability

From the discussion so far, we conclude that for low energy EM wave (here $\hbar\omega = 0.1$ eV), the asborption can be tuned by tuning the E_F. If we change the E_F from $E_F > 0.4$ eV to zero, nearly perfect switching of the reflected EM wave can be observed. This tunability can be used to design an EM wave switching device as shown in Fig. 4.4. The EM wave switching device is a device that can turn on and turn off EM wave at certain point.

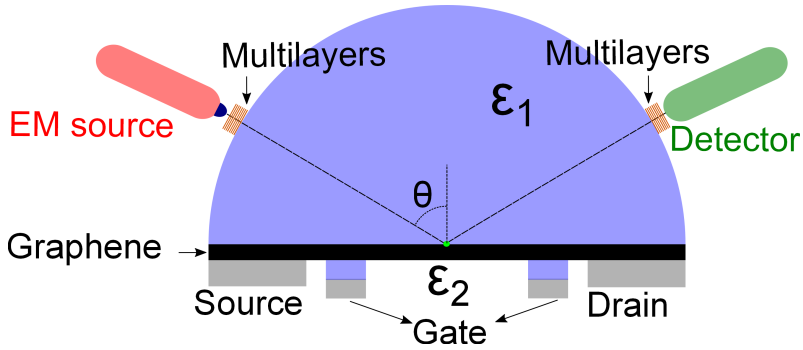

Figure 4.4 Possible design of an EM wave switching device. Multilayered films near the EM wave source and detector are put for avoiding unnecessary reflection.

Fig. 4.4: Fig/fig4k4.eps

In Fig. 4.4, a possible design for an EM wave switching device which consists of an EM wave source, a detector, a gate-voltage modulation system, and a graphene layer sandwiched between two dielectric materials $(\varepsilon_1, \varepsilon_2)$. The EM wave source is placed at a certain angle where the absorption is maximum when $E_{\rm F} \neq 0$. The detector is used to catch the reflected wave. It is necessary to put multi-layered thin films at the interfaces which are attached to medium 1 and are placed in front of the EM wave source and the detector so as to suppress unnecessary reflections at the surface of the medium 1. The most important part is the gates. The gates in the device are used to change $E_{\rm F}$ of monolayer graphene. For instance, we may use electrochemical doping if the medium 1 is an electrolyte material [57].

To use this device, we need to refer to absorption spectrum such as shown in Fig. 4.3(b). The angle of incidence (θ) that we choose should be the one that gives maximal absorption at certain $E_{\rm F}$. For example, in case of $\varepsilon_1 = 2.25$ and $\varepsilon_2 = 1.25$, we will have absorption spectra in Fig. 4.3(b), and if we choose $E_{\rm F} = 0.4$ eV, the θ is 79°. Almost all of EM wave is absorbed by graphene and detector will not detect any EM wave. We assign binary number 0 for this. However, if we change $E_{\rm F}$ to be 0 eV, most of EM wave is reflected by graphene and detected by detector. We assign binary number 1 for this. Thus, we have switching phenomenon for EM wave with low energy.

4.3 Surface plasmon excitation

From previous discussion, we conclude that graphene can absorb almost all of EM wave coming to it provided we have TIR geometry. The EM wave that can be absorbed almost totally should have low energy. Therefore, we need to know the frequency range of the EM wave that can be used for this phenomenon. In order to investigate the frequency range for high absorption of the EM wave, we plot the absorption as function of frequency and angle of incidence as shown in Fig. 4.5.

In Fig. 4.5, the absorption spectrum as function of frequency (f) and angle of incidence (θ) is plotted. We still use the previous configuration, $\varepsilon_1 = 2.25$ and $\varepsilon_2 = 1.25$ and $E_{\rm F} = 0.64$ eV. $\theta_c = 48.19°$, therefore TIR occurs when $\theta > \theta_c$. As we can

Fig. 4.5: Fig/fig4k5br.eps

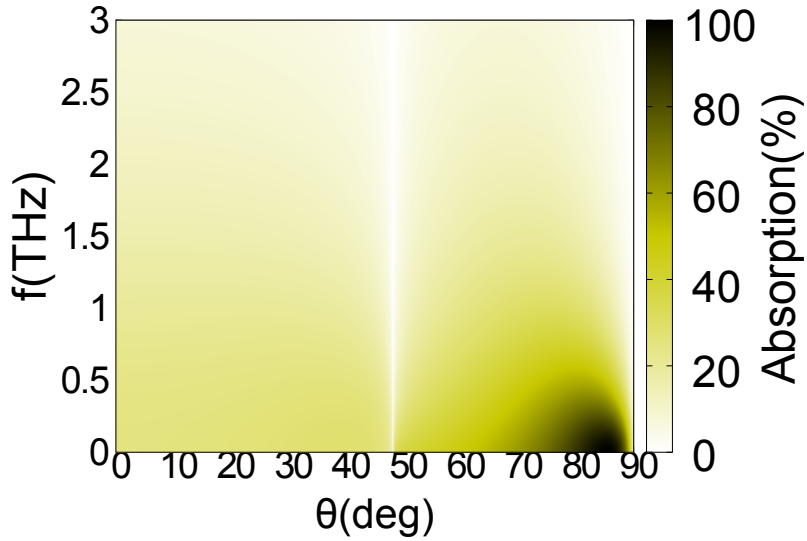

Figure 4.5 Reflectance spectrum as function of frequency (f) and angle of incidence (θ). $\varepsilon_1 = 2.25$ and $\varepsilon_2 = 1.25$ and $E_{\mathrm{F}} = 0.64$ eV. $\theta_c = 48.19°$. The black color means high absorption.

see, the high absorption can only obtained for low frequency and $\theta \sim 80°$. At around $f = 0.3$ THz, the maximum absorption is already around 80 %.

We argue that this high absorption is related to the excitation of low energy SP. To explain this argument, we need to know the dispersion relation of SP at low frequency (or equivalently at small q). We know from Eq. (3.8), for small q ($q \ll k_F$), the SP frequency is a function of $\sqrt{q}$. Eq. (3.8) is also only valid for $\varepsilon_1 = 1$ and $\varepsilon_2 = 1$. Therefore, we need to derive SP dispersion if we have $\varepsilon_1 = 2.25$ and $\varepsilon_2 = 1.25$. To obtain it, we use the semi-classical method. This method is called as semi-classic because it uses the classical Maxwell equations, but the conductivity that is used in the calculation comes from Eq. (4.12), which is derived from quantum mechanics (RPA) calculation. The resulted dispersion will match with the RPA dispersion only at $q \ll k_F$. For $E_{\mathrm{F}} = 0.64$ eV, $k_F = 0.0972\text{Å}^{-1}$. It will also be shown that if we go to smaller q (q is really close to 0), the dispersion will not be a function of $\sqrt{q}$, instead it will be linear to q as shown in the inset of Fig. 4.6.

We use Fig. 4.1, but disregard the external EM fields. Graphene is located at z=0. We consider SP plasmon occurs on graphene and the fields inside ε_1 and ε_2 are graphene SP plasmon's fields. Those fields can be written as

For z < 0

$$E_x^{(1)} = A_1 e^{\kappa_1 z} e^{iqx}$$
$$H_y^{(1)} = \frac{i\omega\varepsilon_0\varepsilon_1}{\kappa_1} A_2 e^{\kappa_1 z} e^{iqx} \quad . \tag{4.13}$$

For z > 0

$$E_x^{(2)} = A_2 e^{-\kappa_2 z} e^{iqx}$$
$$H_y^{(2)} = -\frac{i\omega\varepsilon_0\varepsilon_2}{\kappa_2} A_2 e^{-\kappa_2 z} e^{iqx} \quad , \tag{4.14}$$

where we define $H_y^{(k)} = i\omega\varepsilon_0\varepsilon_k \int E_x^{(k)} dz$. κ is decay constant of SP field in z-direction $\kappa_k = \sqrt{q^2 - \varepsilon_k \frac{\omega^2}{c^2}}$. κ_k value is real, since SP requires decaying fields inside of both media, otherwise we have a propagating field in z-direction. We use the boundary conditions, which are similiar to Eqs. (4.1-4.2). We obtain

$$\frac{\varepsilon_1}{\kappa_1} + \frac{\varepsilon_2}{\kappa_2} + \frac{i\sigma}{\omega\varepsilon_0} = 0 \tag{4.15}$$

We need to solve Eq. 4.15 for $\omega(q)$. The conductivity that is used is just Drude conductivity σ_D, because σ_D is dominant at $\hbar\omega \ll E_{\mathrm{F}}$. The solution is calculated numerically and is plotted in Fig. 4.6.

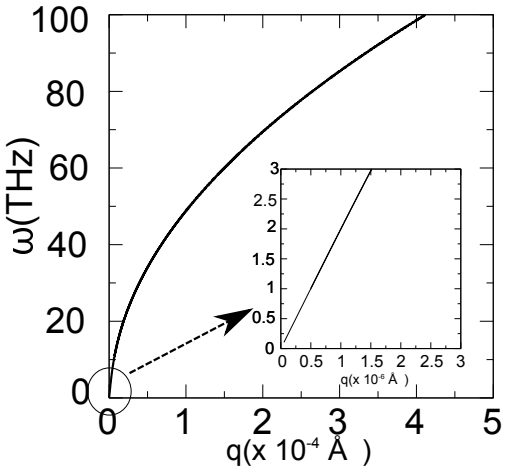

Figure 4.6 SP dispersion obtained by solving Eq. 4.15. At very small ω and q, the dispersion is linear to q and is shown by the inset.

Fig. 4.6: Fig/fig4k6.eps

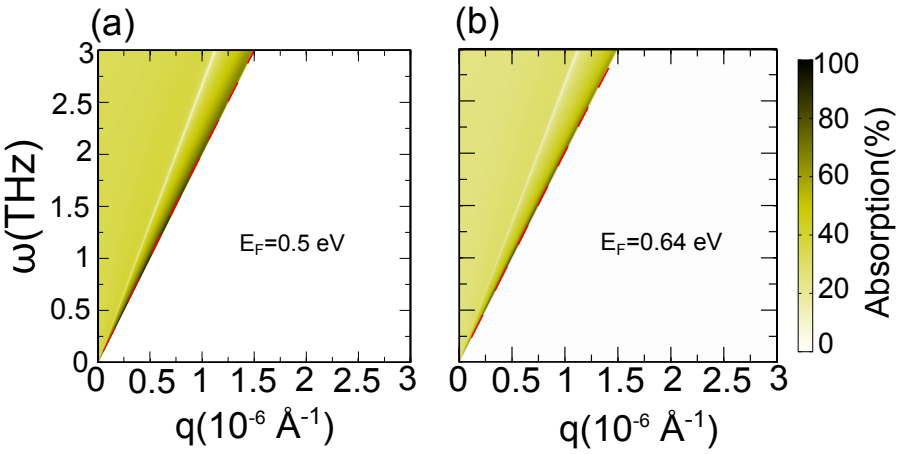

Figure 4.7 (a) The absorption spectrum as function of ω and q for $E_{\mathrm{F}} = 0.5$ eV and $E_{\mathrm{F}} = 0.64$ eV, these plots are to be compared with SP dispersion (the red dash line).

Fig. 4.6 shows the SP dispersion, which is obtained by solving Eq. (4.15) for $\omega(q)$. From the plot, we see the resulted dispersion is a function of $\sqrt{q}$, just like the result obtained from RPA calculation for $q \ll k_F$. To recover the RPA result of Eq. (3.8), we consider that $q \gg \varepsilon_k \omega/c$. This approximation assumes that there is an instantaneous Coulomb coupling between charge [58]. This approximation is called as non-retarded SP. We will have $q = \kappa_k$. Γ is also removed from conductivity in Eq. 4.12. Solving Eq. (4.15), we will arrive at the SP frequency ω

$$\omega = \frac{1}{\hbar}\sqrt{\frac{E_F e^2 q}{\pi\varepsilon_0(\varepsilon_1+\varepsilon_2)}} \quad . \tag{4.16}$$

If we set $\varepsilon_1 = \varepsilon_2 = 1$, we will recover the SP frequency as in Eq. 3.8. If we solve exactly for smaller ω and q, the dispersion actually becomes linear to q. This regime is called retardation regime [58]. In this regime q is comparable to $\varepsilon_k \omega/c$, that is why we need to solve Eq. 4.15 exactly. The exact solution of this regime is linear to q [58] as shown in inset of Fig. 4.6.

Let us go back to the discussion of high EM wave absorption by graphene. To know the origin of this high absorption, we plot the absorption spectrum as function of ω and wave vector of EM wave parallel to graphene surface. It is also denoted by q.

Fig. 4.7: Fig/fig4k7br.eps

Fig. 4.7 shows the absorption spectrum as function of ω and q. We see that the high absorption (black) occupies a line, which is linear to q. If we compare to SP dispersion at the same ω and q scale in Fig. 4.7 (red dash line), we can see that high absorption resides along the SP dispersion. This means that the high absorption of EM wave with very low frequency is due to excitation of graphene SP with very low frequency and wave vector. There is a strong coupling between EM wave with graphene [58], this coupling excites SP and can be observed as high absorption of low energy EM wave . Thus, this is the reason, why we have large absorption of the EM wave.

Chapter 5

Conclusions

Graphene surface plasmon (SP) dispersion is determined by the zero values of real part of dielectric function of graphene. It has been shown in the present thesis that only doped graphene can support SP. We found that undoped graphene does not support SP because real part of dielectric function is always positive. However, in region of non zero of imaginary part of polarization, SP can experience damping due to single electron excitation or known as Landau's damping. Dielectric function of graphene can also be used to calculate the conductivity. Real part of conductivity governs the absorption of electromagnetic (EM) wave. We shows that graphene can absorb almost 100% of incoming EM wave provided that we have low EM wave energy (up to $\omega = 1$ THz) and total internal reflection geometry, in which graphene is placed between two dielectric media. We argue that the high absorption is related to the excitation of SP with low frequency and small wave vector. The absorption probability is also tuneable by changing the Fermi energy (E_{F}). The absorption probability almost vanishes if $E_{\mathrm{F}} = 0$ eV. This behavior can be utilized for designing a EM wave switching device controlled by gate voltage.

Within this thesis, we have derived the dielectric function of graphene, the graphene SP dispersion and its damping, and also we have obtained and discussed the absorption spectra of EM wave in graphene. The missing thing is the calculation of energy dissipation of EM wave coming to graphene. This will be interesting subject for our future study.

Appendix A

Derivation of Graphene Dielectric Function

Here we give more detailed derivation of some calculations of graphene dielectric function that are not explained in deep within the main thesis content.

A.0.1 Overlap of electron wave function in Dirac cone

Here we give detailed derivation of electron wave function overlap within the Dirac cone. It is denoted as $F_{ss'} = |\langle sk|s'k+q\rangle|^2$. The wave functions are expressed in Eq. (2.17) and (2.18).

$$\begin{aligned} F_{ss'} =& \frac{1}{4}\left|\left(e^{i(\theta_k-\theta_{k+q})/2} + ss'e^{-i(\theta_k-\theta_{k+q})/2}\right)\right|^2 \\ =& \frac{1}{4}\left|e^{i\theta/2} + ss'e^{-i\theta/2}\right|^2 \\ =& \frac{1}{2}(ss'\cos\theta + 1) \quad . \end{aligned} \tag{A.1}$$

Here $\theta = \theta_k - \theta_{k+q}$. We want expression in term of ϕ, that is angle between q and

k ($\phi = \theta_q - \theta_k$). What we need to change is $\cos\theta$.

$$\begin{aligned}
\cos\theta =& \cos(\theta_{k+q} - \theta_k) \\
=& \cos\theta_{k+q}\cos\theta_k + \sin\theta_{k+q}\sin\theta_k \\
=& \frac{(\mathbf{k}+\mathbf{q})_x}{|\mathbf{k}+\mathbf{q}|}\cos\theta_k + \frac{(\mathbf{k}+\mathbf{q})_y}{|\mathbf{k}+\mathbf{q}|}\sin\theta_k \\
=& \frac{k\cos\theta_k + q\cos\theta_q}{|\mathbf{k}+\mathbf{q}|}\cos\theta_k + \frac{k\sin\theta_k + q\sin\theta_q}{|\mathbf{k}+\mathbf{q}|}\sin\theta_k \\
=& \frac{k + q(\cos\theta_q\cos\theta_k + \sin\theta_q\sin\theta_k)}{|\mathbf{k}+\mathbf{q}|} \\
=& \frac{k + q\cos\phi}{|\mathbf{k}+\mathbf{q}|} \quad . \qquad \text{(A.2)}
\end{aligned}$$

We use the fact that,

$$\begin{aligned}
(\mathbf{k}+\mathbf{q})_x =& k_x + q_x \\
=& k\cos\theta_k + q\cos\theta_q \qquad \text{(A.3)} \\
(\mathbf{k}+\mathbf{q})_y =& k_y + q_y \\
=& k\sin\theta_k + q\sin\theta_q \qquad \text{(A.4)}
\end{aligned}$$

A.0.2 Delta function integration

Integrations involving delta function (δ-function) are done many times within our discussion of the main thesis. For instance, Eq. (2.39), the integration on ϕ involves δ-function. The integration is changed first into on $\cos\phi$ by substitution and also the δ-function is changed in term of $\cos\phi$ by using delta function property : $\delta(f(x)) = \sum_i \delta(x - x_i)/|\frac{\partial f(x)}{\partial x}|_{x_i}$.

$$\delta(\omega - v_{\mathrm{F}}k - v_{\mathrm{F}}|\mathbf{k}+\mathbf{q}|) = \delta(\omega - v_{\mathrm{F}}k - v_{\mathrm{F}}\left(k^2 + q^2 + 2kq\cos\phi\right)^{\frac{1}{2}}) \quad . \qquad \text{(A.5)}$$

We want the δ-function in term of $\cos\phi$. Therefore we need to find its root (x_i). The root can be obtained from the zero of δ-function argument.

$$\begin{aligned}
\omega - v_{\mathrm{F}}k =& v_{\mathrm{F}}\sqrt{k^2 + q^2 + 2kq\cos\phi} \\
\cos\phi_i =& \frac{\omega^2 - 2v_{\mathrm{F}}k\omega - v_{\mathrm{F}}^2q^2}{2v_{\mathrm{F}}^2kq} \quad . \qquad \text{(A.6)}
\end{aligned}$$

We have found the root $\cos\phi_i$. The value of $|\mathbf{k}+\mathbf{q}|$ evaluated with the root can be obtained also from the zero δ-function argument, $|\mathbf{k}+\mathbf{q}| = \frac{\omega - v_{\mathrm{F}}k}{v_{\mathrm{F}}}$. The derivative of δ-function evaluated with the root can be calculated.

$$f(\cos\phi) = \omega - v_{\mathrm{F}}k - v_{\mathrm{F}}\left(k^2+q^2+2kq\cos\phi\right)^{\frac{1}{2}}$$
$$|\frac{\partial f(\cos\phi)}{\partial\cos\phi}|_{\cos\phi_i} = \frac{v_{\mathrm{F}}kq}{|\mathbf{k}+\mathbf{q}|} \quad . \tag{A.7}$$

We have transformed δ-function to be in term of $\cos\phi$.

$$\delta(\omega - v_{\mathrm{F}}k - v_{\mathrm{F}}|\mathbf{k}+\mathbf{q}|) = \frac{|\mathbf{k}+\mathbf{q}|}{v_{\mathrm{F}}kq}\delta\left(\cos\phi - \frac{\omega^2 - 2v_{\mathrm{F}}k\omega - v_{\mathrm{F}}^2q^2}{2v_{\mathrm{F}}^2kq}\right) \quad . \tag{A.8}$$

The integration is changed to be on $\cos\phi$ instead of ϕ.

$$\int_0^{2\pi} d\phi = \int_0^{\pi} d\phi + \int_{\pi}^{2\pi} d\phi \tag{A.9}$$
$$= -\int_1^{-1} \frac{d(\cos\phi)}{\sin\phi} - \int_{-1}^{1} \frac{d(\cos\phi)}{\sin\phi} \tag{A.10}$$
$$= \int_{-1}^{1} \frac{d(\cos\phi)}{|\sin\phi|} + \int_{-1}^{1} \frac{d(\cos\phi)}{|\sin\phi|} \tag{A.11}$$
$$= 2\int_{-1}^{1} \frac{d(\cos\phi)}{|\sin\phi|} \tag{A.12}$$

The second term in Eq. A.10 is in third and forth quadrant where $\sin\phi$ is negative. Therefore $\sin\phi$ is change to be its absolute value $|\sin\phi|$ and we have Eq. (A.11) and the negative signs become positive. Now we have Eq. (2.39). To solve the δ-function integration in Eq. (2.39), we just need to substitute $\cos\phi = \frac{\omega^2 - 2v_{\mathrm{F}}k\omega - v_{\mathrm{F}}^2q^2}{2v_{\mathrm{F}}^2kq}$, $|\mathbf{k}+\mathbf{q}| = \frac{\omega - v_{\mathrm{F}}k}{v_{\mathrm{F}}}$ and $\sin\phi = \sqrt{1-\cos^2\phi}$. Finally, we will have Eq. (2.40).

In Eq. (2.40), we make some simplification of the equation. It will be derived below.

$$
\begin{aligned}
\operatorname{Im}\Pi_{0g}(q,\omega) &= -\frac{1}{\pi\hbar}\int dk \frac{v_{\mathrm{F}}^2q^2-(\omega-2v_{\mathrm{F}}k)^2}{v_{\mathrm{F}}\sqrt{(2v_{\mathrm{F}}^2kq)^2-(\omega^2-2v_{\mathrm{F}}k\omega-v_{\mathrm{F}}^2q^2)^2}} \\
&= -\frac{1}{\pi\hbar}\int dk \frac{v_{\mathrm{F}}^2q^2-(\omega-2v_{\mathrm{F}}k)^2}{v_{\mathrm{F}}\sqrt{4v_{\mathrm{F}}^4k^2q^2-\omega^2(\omega-2v_{\mathrm{F}})^2+2\omega^2v_{\mathrm{F}}^2q^2-4\omega v_{\mathrm{F}}^3kq^2-(v_{\mathrm{F}}^2q^2)^2}} \\
&= -\frac{1}{\pi\hbar}\int dk \frac{v_{\mathrm{F}}^2q^2-(\omega-2v_{\mathrm{F}}k)^2}{v_{\mathrm{F}}\sqrt{-\omega^2(\omega-2v_{\mathrm{F}}k)^2+\omega^2v_{\mathrm{F}}^2q^2+v_{\mathrm{F}}^2q^2(\omega^2-4\omega v_{\mathrm{F}}k+4\omega v_{\mathrm{F}}^2k^2)-(v_{\mathrm{F}}^2q^2)^2}} \\
&= -\frac{1}{\pi\hbar}\int dk \frac{v_{\mathrm{F}}^2q^2-(\omega-2v_{\mathrm{F}}k)^2}{v_{\mathrm{F}}\sqrt{-\omega^2(\omega-2v_{\mathrm{F}}k)^2+\omega^2v_{\mathrm{F}}^2q^2+v_{\mathrm{F}}^2q^2(\omega-2v_{\mathrm{F}}k)^2-(v_{\mathrm{F}}^2q^2)^2}} \\
&= -\frac{1}{\pi\hbar}\int dk \frac{v_{\mathrm{F}}^2q^2-(\omega-2v_{\mathrm{F}}k)^2}{v_{\mathrm{F}}\sqrt{\omega^2(v_{\mathrm{F}}^2q^2-(\omega-2v_{\mathrm{F}}k)^2)-v_{\mathrm{F}}^2q^2(v_{\mathrm{F}}^2q^2-(\omega-2v_{\mathrm{F}}k)^2)}} \\
&= -\frac{1}{\pi\hbar}\int dk \frac{v_{\mathrm{F}}^2q^2-(\omega-2v_{\mathrm{F}}k)^2}{v_{\mathrm{F}}\sqrt{(v_{\mathrm{F}}^2q^2-(\omega-2v_{\mathrm{F}}k)^2)(\omega^2-v_{\mathrm{F}}^2q^2)}} \\
&= -\frac{1}{\pi\hbar}\frac{1}{v_{\mathrm{F}}\sqrt{\omega^2-v_{\mathrm{F}}q^2}}\int dk\sqrt{v_{\mathrm{F}}^2q^2-(\omega-2v_{\mathrm{F}}k)^2} \quad . \qquad \text{(A.13)}
\end{aligned}
$$

A.0.3 Real part of doped graphene polarization

In this section, we will give a more detailed derivation for getting the $\operatorname{Re}\Pi_{0g}(q,\omega)$. We first take a look at Eq. (2.53). Here, the real part of polarization is split by index α. The nominator of Eq. (2.53) becomes step function $-\alpha\theta(k-\frac{E_{\mathrm{F}}}{\hbar v_{\mathrm{F}}})$. In order to calculate directly, we change the index: $n_{\alpha,k}-n_{\alpha\beta,k+q}\longrightarrow n_{\alpha,k}-n_{-\alpha,k}$. There are 4 possibilities of $n_{\alpha,k}-n_{-\alpha,k}$ value.

If $k > \frac{E_{\mathrm{F}}}{\hbar v_{\mathrm{F}}}$. For $\alpha=1$

$$n_{+,k}-n_{-,k}=0-1=-1 \quad . \qquad \text{(A.14)}$$

For $\alpha=-1$

$$n_{-,k}-n_{+,k}=1-0=1 \quad . \qquad \text{(A.15)}$$

If $k < \frac{E_{\mathrm{F}}}{\hbar v_{\mathrm{F}}}$. For $\alpha=1$

$$n_{+,k}-n_{-,k}=1-1=0 \quad . \qquad \text{(A.16)}$$

For $\alpha=-1$

$$n_{-,k}-n_{+,k}=1-1=0 \quad . \qquad \text{(A.17)}$$

From these possibilities, we can conclude that $n_{\alpha,k} - n_{-\alpha,k} = -\alpha\theta(k - \frac{E_F}{\hbar v_F})$. Therefore, the real part of polarization can be written as,

$$\begin{aligned}
\mathrm{Re}\,\Pi_{0g}(q,\omega) =& \frac{2}{A}\sum_{k,\alpha,\beta}\frac{-\alpha\theta(k-\frac{E_F}{\hbar v_F})}{\hbar\omega+\alpha(\hbar v_F k-\hbar v_F\beta|\mathbf{k}+\mathbf{q}|)}\left(1+\frac{k+q\cos\phi}{|\mathbf{k}+\mathbf{q}|}\right)\\
=& \frac{2}{A}\sum_{k,\alpha,\beta}\frac{-\alpha\theta(k-\frac{E_F}{\hbar v_F})}{\hbar\omega+\alpha\hbar v_F k-\hbar v_F\alpha\beta|\mathbf{k}+\mathbf{q}|}\left(1+\frac{k+q\cos\phi}{|\mathbf{k}+\mathbf{q}|}\right)\\
&\times\frac{\omega+\alpha v_F k+v_F\alpha\beta|\mathbf{k}+\mathbf{q}|}{\omega+\alpha v_F k+v_F\alpha\beta|\mathbf{k}+\mathbf{q}|}\\
=& \frac{2}{A\hbar}\sum_{k,\alpha,\beta}\frac{-\alpha\theta(k-\frac{E_F}{\hbar v_F})(\omega+\alpha v_F k+v_F\alpha\beta|\mathbf{k}+\mathbf{q}|)}{\omega^2-v_F^2q^2+2kv_F\omega\alpha-2kv_F^2q\cos\phi}\left(1+\frac{k+q\cos\phi}{|\mathbf{k}+\mathbf{q}|}\right)\\
=& \frac{2}{A\hbar}\sum_{k,\alpha,\beta}\left[-\alpha\theta(k-\frac{E_F}{\hbar v_F})\left\{\omega+2\alpha v_F k+\alpha v_F q\cos\phi\right.\right.\\
&\left.\left.+\beta\left(\frac{\alpha|\mathbf{k}+\mathbf{q}|+(\omega+\alpha k)(k+q\cos\phi)}{|\mathbf{k}+\mathbf{q}|}\right)\right\}\right]\\
&\times\frac{1}{\omega^2-v_F^2q^2+2kv_F\omega\alpha-2kv_F^2q\cos\phi}\\
=& \frac{4}{A\hbar}\sum_{k,\alpha}\frac{-\alpha\theta(k-\frac{E_F}{\hbar v_F})(\omega+2\alpha v_F k+\alpha v_F q\cos\phi)}{\omega^2-v_F^2q^2+2kv_F\omega\alpha-2kv_F^2q\cos\phi}\\
=& \frac{2}{A\hbar}\sum_{k,\alpha}\frac{-2\alpha\omega-4\alpha^2v_F k-2v_F q\cos\phi}{\omega^2-v_F^2q^2+2kv_F\omega\alpha-2kv_F^2q\cos\phi}\theta(k-\frac{E_F}{\hbar v_F})\\
=& \frac{1}{2\pi^2\hbar}\sum_{\alpha}\int dk\theta(k-\frac{E_F}{\hbar v_F})\frac{v_F}{v_F}k\int_0^{2\pi}d\phi\frac{-2\alpha\omega-4\alpha^2v_F k-2v_F q\cos\phi}{\omega^2-v_F^2q^2+2kv_F\omega\alpha-2kv_F^2q\cos\phi}
\end{aligned} \tag{A.18}$$

We need to modify the integrand, so that the integration can be solved more easily. Suppose we want to have

$$\begin{aligned}
1+B =& \frac{-2v_F\alpha\omega-4\alpha^2v_F^2k-2v_F^2q\cos\phi}{\omega^2-v_F^2q^2+2kv_F\omega\alpha-2kv_F^2q\cos\phi}\\
B =& \frac{-2\alpha\omega-4\alpha^2v_F k-2v_F q\cos\phi}{\omega^2-v_F^2q^2+2kv_F\omega\alpha-2kv_F^2q\cos\phi}-1\\
=& \frac{v_F^2q^2-(2v_F k+\alpha\omega)^2}{\omega^2-v_F^2q^2+2kv_F\omega\alpha-2kv_F^2q\cos\phi}\quad .
\end{aligned} \tag{A.19}$$

Substituting back $1+B$ to Eq. (A.18), we will have Eq. (2.53). The function in the nominator is not a function of ϕ anymore. The integration on ϕ of Eq. (2.53) can now readily be executed. We will use complex plane integration in form of :

$$\begin{aligned}\int_0^{2\pi} \frac{d\phi}{a+b\cos\phi} =& \oint \frac{1}{a+\frac{b}{2}(z+z^{-1})}\frac{dz}{iz} \\ =& \frac{2}{ib}\oint \frac{dz}{z^2+\frac{2a}{b}z+1} \\ =& \frac{2}{ib}\oint \frac{dz}{\left\{z-\left(-\frac{a}{b}+\frac{1}{b}\sqrt{a^2-b^2}\right\}\right)\left\{z-\left(-\frac{a}{b}-\frac{1}{b}\sqrt{a^2-b^2}\right)\right\}} \quad . \end{aligned} \tag{A.20}$$

If $a > |b|$, the pole is $\left(-\frac{a}{b}+\frac{1}{b}\sqrt{a^2-b^2}\right)$.

$$\begin{aligned}\int_0^{2\pi} \frac{d\phi}{a+b\cos\phi} =& \frac{4\pi}{b}\frac{1}{\left\{\left(-\frac{a}{b}+\frac{1}{b}\sqrt{a^2-b^2}\right\}-\left\{-\frac{a}{b}-\frac{1}{b}\sqrt{a^2-b^2}\right)\right\}} \\ =& \frac{2\pi}{\sqrt{a^2-b^2}} \quad . \end{aligned} \tag{A.21}$$

If $-a > |b|$, the pole is $\left(-\frac{a}{b}-\frac{1}{b}\sqrt{a^2-b^2}\right)$.

$$\begin{aligned}\int_0^{2\pi} \frac{d\phi}{a+b\cos\phi} =& \frac{4\pi}{b}\frac{1}{\left\{\left(-\frac{a}{b}-\frac{1}{b}\sqrt{a^2-b^2}\right\}-\left\{-\frac{a}{b}+\frac{1}{b}\sqrt{a^2-b^2}\right)\right\}} \\ =& -\frac{2\pi}{\sqrt{a^2-b^2}} \quad . \end{aligned} \tag{A.22}$$

We define $z = e^{i\phi}$ and $\cos\phi = \frac{z+z^{-1}}{2}$. Therefore, the contour on complex plane is unit circle. To use this results, the integration on ϕ of Eq. (2.53), we substitute $a = \omega^2 - v_{\mathrm{F}}^2 a^2 + 2kv_{\mathrm{F}}\omega\alpha$ and $b = -2kv_{\mathrm{F}}^2 q$. The integration depends on α. We start with $\alpha = -1$, there are two possibilities of ω, $\omega > v_{\mathrm{F}}q$ and $\omega < v_{\mathrm{F}}q$. For first case, we consider $\omega > v_{\mathrm{F}}q$. In this case, if we consider $-a > |b|$, we arrive at quadratic inequality of $\omega^2 - v_{\mathrm{F}}^2 q^2 - 2kv_{\mathrm{F}}\omega + 2kv_{\mathrm{F}}^2 q < 0$. We will obtain constraint on k, that is $k > \frac{\omega+v_{\mathrm{F}}q}{2v_{\mathrm{F}}}$. If we consider $a > |b|$, we arrive at quadratic inequality of $\omega^2 - v_{\mathrm{F}}^2 q^2 - 2kv_{\mathrm{F}}\omega - 2kv_{\mathrm{F}}^2 q > 0$ and we will obtain constraint on k, that is $k < \frac{\omega-v_{\mathrm{F}}q}{2v_{\mathrm{F}}}$. For second case, we consider $\omega < v_{\mathrm{F}}q$. In this case, we always have $a < |b|$ for every k value, however, we can have $-a > |b|$. This gives us quadratic inequality of $\omega^2 - v_{\mathrm{F}}^2 q^2 - 2kv_{\mathrm{F}}\omega + 2kv_{\mathrm{F}}^2 q < 0$. This gives us $k < \frac{\omega+v_{\mathrm{F}}q}{2v_{\mathrm{F}}}$. The results of integration for case of $-a > |b|$ and $a > |b|$ are given in Eq. (A.21) and (A.22).

We now look at $\alpha = 1$. For first case $\omega > v_{\mathrm{F}}q$, we always have $a > |b|$ for every k value. For second case $\omega < v_{\mathrm{F}}q$, we always have $a < |b|$ for every k value, however, we can have $-a > |b|$. This gives us quadratic inequality of

$\omega^2 - v_{\rm F}^2 q^2 + 2kv_{\rm F}\omega + 2kv_{\rm F}^2 q < 0$. Therefore, we have contraint on k to be $k < \frac{\omega + v_{\rm F} q}{2v_{\rm F}}$. The results of integration for case of $-a > |b|$ and $a > |b|$ are given in Eq. (A.21) and (A.22).

The constraints on k yield the step function in Eq. (2.54) and (2.55). This step function will determine the boundary of integration on k.

Appendix B

Plasmon Dispersion and Damping Constant

B.1 Plasmon dispersion and damping constant formula

Here we will give more detailed derivation of Eq. (3.2) and (3.3) in chapter (3). From Eq. (3.2), plasmon dispersion relation can be obtained and from Eq. (3.3), damping constant of plasmon can be obtained. Both of them actually come from Eq. (3.1). The zeroes of Eq. (3.1) are the solutions of plasmon. The zeroes of Eq. (3.1) should satisfy

$$1 = \frac{e^2}{2\varepsilon_0 q}\Pi_{0g}(q, \Omega - i\gamma) \quad , \tag{B.1}$$

Where SP can occur at $\omega = \Omega - i\gamma$ of Eq. 3.1. What we need to do is to separate Eq. B.1 into real and imaginary parts. We define that

$$f_p = \frac{e^2}{2\varepsilon_0 q}\Pi_{0g}(q, \omega) \quad . \tag{B.2}$$

We can seperate the f_p into real and imaginary parts.

$$\text{Re } f_p + i \text{ Im } f_p = \frac{e^2}{2\varepsilon_0 q}\text{Re } \Pi_{0g}(q, \omega) + i \ \frac{e^2}{2\varepsilon_0 q}\text{Im } \Pi_{0g}(q, \omega) \quad . \tag{B.3}$$

Taking Taylor expansion of Re $\Pi_{0g}(q, \omega)$ around $\omega = \Omega - i\gamma$, we will have

$$\begin{aligned}\text{Re } f_p + i \text{ Im } f_p =& \frac{e^2}{2\varepsilon_0 q}\text{Re } \Pi_{0g}(q, \Omega - i\gamma) + \frac{e^2}{2\varepsilon_0 q}\left[\frac{\partial \text{Re } \Pi_{0g}(q, \Omega - i\gamma)}{\partial \omega}\right]_{\omega=\Omega-i\gamma} \\ & \times (\omega - \Omega + i\gamma) + i \ \frac{e^2}{2\varepsilon_0 q}\text{Im } \Pi_{0g}(q, \omega) \quad .\end{aligned} \tag{B.4}$$

From Eq. (B.4), we can separate the the f_p into real and imaginary parts. We assume that $\gamma \ll \Omega$.

$$\text{Re } f_p = \frac{e^2}{2\varepsilon_0 q}\text{Re } \Pi_{0g}(q,\Omega) + \frac{e^2}{2\varepsilon_0 q}\left[\frac{\partial \text{Re } \Pi_{0g}(q,\omega)}{\partial\omega}\right]_{\omega=\Omega}(\omega-\Omega) \quad . \tag{B.5}$$

$$\text{Im } f_p = \frac{e^2}{2\varepsilon_0 q}\text{Im } \Pi_{0g}(q,\Omega) + \gamma\frac{e^2}{2\varepsilon_0 q}\left[\frac{\partial \text{Re } \Pi_{0g}(q,\omega)}{\partial\omega}\right]_{\omega=\Omega} \quad . \tag{B.6}$$

At $\omega = \Omega - i\gamma(\gamma \ll \Omega)$, we have Re $f_p = 1$ and Im $f_p = 0$. From this, we can have Eq. (3.2) and (3.3) from Eq. (B.5) and (B.6), respectively. We just take the absolute value of γ.

B.2 Plasmon dispersion plot

In plotting the plasmon disperison relation, we make use of scaling of frequency and wave vector. The energy (hence the frequency) is scaled with respect to Fermi energy (E_F) and wave vector is scaled with respect to Fermi wave vector (k_F).

The plot of polarization and dielectric function (Figure 2.7, 2.6, 2.7) are function of $\frac{\hbar\omega}{E_\text{F}}$ and $\frac{q}{k_\text{F}}$. To plot them, the expression of polarization should be scaled.

We assume that $W = \frac{\hbar\omega}{E_\text{F}}$ and $Q = \frac{q}{k_\text{F}}$. First we scale the real part of polarization in Eq. (2.56).

$$\begin{aligned}
\text{Re}\,\Pi_{0g}(Q,W) =& \frac{E_\text{F}}{\pi\hbar^2 v_\text{F}^2}\Bigg[-2 + \frac{Q^2}{4}\frac{\theta(W-Q)}{\sqrt{W^2-Q^2}}\Bigg\{g\left(\frac{W+2}{Q}\right) \\
&- \theta\left(\frac{W-Q}{2}-1\right)g\left(\frac{W-2}{Q}\right) \\
&+ \theta\left(1-\frac{W+Q}{2}\right)g\left(\frac{2-W}{Q}\right)\Bigg\} \\
&- \frac{Q^2}{4}\frac{\theta(Q-W)}{\sqrt{Q^2-W^2}}\Bigg\{\theta\left(\frac{W+Q}{2}-1\right) \\
&\times\left(f(1)-f\left(\frac{2-W}{Q}\right)\right) + \theta\left(\frac{Q-W}{2}-1\right) \\
&\times\left(f(1)-f\left(\frac{W+2}{Q}\right)\right)\Bigg\}\Bigg] \quad .
\end{aligned} \tag{B.7}$$

The value of real part of polarization depends on E_{F}. However if we want to plot the real part of dielectric function, the value does not depend on E_{F}.

$$\begin{aligned}\mathrm{Re}\,\varepsilon(Q,W) =& 1-\frac{e^2}{2\varepsilon_0 q}\times\frac{E_{\mathrm{F}}}{\pi\hbar^2 v_{\mathrm{F}}^2}\Bigg[-2+\frac{Q^2}{4}\frac{\theta(W-Q)}{\sqrt{W^2-Q^2}}\Bigg\{g\left(\frac{W+2}{Q}\right)\\ &-\theta\left(\frac{W-Q}{2}-1\right)g\left(\frac{W-2}{Q}\right)\\ &+\theta\left(1-\frac{W+Q}{2}\right)g\left(\frac{2-W}{Q}\right)\Bigg\}\\ &-\frac{Q^2}{4}\frac{\theta(Q-W)}{\sqrt{Q^2-W^2}}\Bigg\{\theta\left(\frac{W+Q}{2}-1\right)\\ &\times\left(f(1)-f\left(\frac{2-W}{Q}\right)\right)+\theta\left(\frac{Q-W}{2}-1\right)\\ &\times\left(f(1)-f\left(\frac{W+2}{Q}\right)\right)\Bigg\}\Bigg]\\ =&1-\frac{e^2}{2Q\varepsilon_0\pi\hbar v_{\mathrm{F}}}\times[-2+...] \quad .\end{aligned} \tag{B.8}$$

The scaling of imaginary part of polarization is shown as follows.

$$\begin{aligned}\mathrm{Im}\,\Pi_{0g}^{\mathrm{inter}}(Q,W) =& -\frac{Q^2E_{\mathrm{F}}}{4\pi\hbar^2v_{\mathrm{F}}^2}\frac{\theta(W-Q)}{\sqrt{W^2-Q^2}}\Bigg[\{f(1)-f(-1)\}\,\theta\left(\frac{W-Q}{2}-1\right)\\ &+\left\{f(1)-f(\frac{2-W}{Q})\right\}\theta\left(1-\frac{W-Q}{2}\right)\theta\left(\frac{W+Q}{2}-1\right)\Bigg] \quad .\end{aligned} \tag{B.9}$$

$$\begin{aligned}\mathrm{Im}\,\Pi_{0g}^{\mathrm{intra}}(Q,W) =& -\frac{Q^2E_{\mathrm{F}}}{4\pi\hbar^2v_{\mathrm{F}}^2}\frac{\theta(W-Q)}{\sqrt{W^2-Q^2}}\Bigg[\left\{g\left(\frac{W+2}{Q}\right)-g(1)\right\}\theta(W-1)\\ &\times\theta\left(1-\frac{Q-W}{2}\right)+\left\{g\left(\frac{W+2}{Q}\right)-g(1)\right\}\theta(1-W)\\ &\times\theta\left(1-\frac{Q-W}{2}\right)\theta\left(\frac{Q+W}{2}-1\right)\\ &+\left\{g\left(\frac{Q+2}{Q}\right)-g\left(\frac{2-W}{Q}\right)\right\}\theta(1-W)\\ &\times\theta\left(1-\frac{Q+W}{2}\right)\Bigg] \quad .\end{aligned} \tag{B.10}$$

The value of imaginary part of polarization depends on E_{F}. However if we want to plot the imaginary part of dielectric function, the value does not depend on E_{F}.

$$\begin{aligned}\operatorname{Im}\varepsilon(Q,W) =& \frac{e^2}{2\varepsilon_0 q} \times \frac{Q^2 E_{\mathrm{F}}}{4\pi\hbar^2 v_{\mathrm{F}}^2} \times ... \\ =& \frac{Qe^2}{8\pi\varepsilon_0 \hbar v_{\mathrm{F}}} \times ...\end{aligned} \tag{B.11}$$

The polarization has unit of $(\mathrm{eV\AA}^2)^{-1}$, while the dielectric function has no unit.

Appendix C

Calculation Program

The expression of dielectric function and conductivity are obtained analytically. Therefore, the programs here are used to plot them. The programs will generate the data files (*.dat), and the data files should be plotted using gnuplot or xmgrace.

All the necessary programs can be found under the following directory in FLEX workstation:

`~shoufie/for/grapplas/`

C.1 Plasmon dispersion plot, gamma and tau

`Program : gamma.f90`

`Inputs :`

range of q and w can be changed. Here we set the range to be 3. q and w here are Q and W defined in Appendix B. Because everything is normalized to E_{F}, so there is no input of E_{F}. Everything is for doped case.

`Outputs :`

1. Real part of dielectric function : the data file is rev.dat. It should be plotted using gnuplot. It will plot Real part of dielectric function as colored plot as function of Q and W. Definition of Q and W explained in Appendix B.

2. Plasmon dispersion plot : the data file is plasmondis.dat. It should be plotted using xmgrace. It will plot W as function of Q.

3. Gamma (damping constant) : the data file is gamma.dat. It should be plotted using xmgrace. It will plot $\hbar\gamma/E_{\mathrm{F}}$ as function of Q. So both of x and y axis are dimensionless.

4. Tau (lifetime) : the data file is tau.dat. It should be plotted using xmgrace. It will plot $\tau E_{\mathrm{F}}/\hbar$ as function of Q. Both of x and y axis are dimensionless.

C.2 Imaginary part of polarization and dielectric function

`Program : dopedim.f90`

`Inputs :`

range of q and w can be changed. Here we set the range to be 3. q and w here are Q and W defined in Appendix B. For plotting the imaginary part of polarization, the $E_{\mathrm{F}} = 1$ eV. For imaginary part of dielectric function, everything is normalized to E_{F}. Everything is for doped case.

`Outputs :`

1. Imaginary part of polarization : the data file is imgdop.dat. It should be plotted using gnuplot. It will plot the imaginary part of polarization as colored plot as function of Q and W. Definition of Q and W explained in Appendix B. For plotting the imaginary part of polarization, the $E_{\mathrm{F}} = 1$ eV.

2. Imaginary part of dielectric function : the data file is rim.dat. It should be plotted using gnuplot. It will plot the imaginary part of dielectric function as colored plot as function of Q and W.

C.3 Absorption, Reflection, Transmission

This program is used to obtain the Absorption, Reflection, Transmission (ART) probabilities as function of angle of incident.

`Program : RTanalytic.f90`

`Inputs :`

Dielectric constants of medium 1 and 2 are defined as eps1 and eps2. E_{F} is defined as ef and frequency as f. The range of incident angle is theta. Everything should be in SI unit.

`Output :`

1. ART : the data file is RT-a.dat. It should be plotted in xmgrace. It will plot the ART probabilities as function of angle of incident.

2. Absorption only : the data file is Absorb-a.dat. It should be plotted in xmgrace. It will plot the absorption probability only as function of angle of incident.

C.4 Absorption spectrum

`Program : speksingle.f90`

`Inputs :`

Dielectric constants of medium 1 and 2 are defined as eps1 and eps2. E_{F} is defined as ef. The range of frequency and incident angle is f and theta. Everything should be in SI unit.

`Output :`

The absorption spectrum : the data file is Spectra-single.dat. It should be plotted using gnuplot. It will plot the absorption spectrum as colored plot as function of frequency and angle of incident.

C.5 Dispersion spectrum

`Program : dispersionsingle.f90`

`Inputs :`

Dielectric constants of medium 1 and 2 are defined as eps1 and eps2. E_{F} is defined as ef. The range of angular frequency and wave vector of EM wave parallel to graphene is w and q. Everything should be in SI unit.

`Output :`

The absorption spectrum : the data file is dispersion.dat. It should be plotted using gnuplot. It will plot the absorption spectrum as colored plot as function of angular frequency and wave vector of EM wave parallel to graphene.

Publication list

Papers

1. **M. S. Ukhtary**, E. H. Hasdeo, A. R. T. Nugraha, R. Saito, Fermi energy-dependence of electromagnetic wave absorption in graphene, APEX, 8, 055102 -1-4, (2015).

Conferences

Oral presentations

1. **M. S. Ukhtary**, E. H. Hasdeo, A. R. T. Nugraha, R. Saito: Plasmons in Graphene. Presented in ATI 2014 Nano-Carbon Meeting and Zao14 Meeting (2015.07.31-08.1), Yamagata-Zao, Japan.

Poster Presentations

1. **M. S. Ukhtary**, E. H. Hasdeo, A. R. T. Nugraha, R. Saito: Propagation Properties of Graphene Surface Plasmons. Presented in the 47rd Fullerene-Nanotubes-Graphene General Symposium (2014.09.03-05), Nagoya University, Japan.

2. **M. S. Ukhtary**, E. H. Hasdeo, A. R. T. Nugraha, R. Saito: Surface Plasmon Excitations in Graphene . Presented in the 48rd Fullerene-Nanotubes-Graphene General Symposium (11-13 March 2013), Tokyo University, Japan.

3. **M. S. Ukhtary**, E. H. Hasdeo, A. R. T. Nugraha, R. Saito: Switching of electromagnetic (EM) wave by graphene. Presented in NT15: The Fourteenth Inter-

national Conference on the Science and Application of Nanotubes (2015.06.28-07.3), Nagoya University, Japan.

Bibliography

[1] R. Saito, G. Dresselhaus, and M. S. Dresselhaus, Physical Properties of Carbon Nanotubes (Imperial College Press, London, 1998).

[2] H-S Philip Wong and Deji Akinwande, Carbon nanotube and graphene device physics (Cambridge University Press, New York, 2010).

[3] Eddwi Hesky Hasdeo. Electronic Raman spectroscopy of metallic carbon nanotubes. Ph. D. thesis, Tohoku University, Department of Physics, June 2013.

[4] Phaedon Avouris, Nano letters 10(11), 4285–4294 (2010).

[5] AH Castro Neto, F Guinea, NMR Peres, Kostya S Novoselov, and Andre K Geim, Reviews of modern physics 81(1), 109 (2009).

[6] KS Novoselov, P Blake, and MI Katsnelson, Encyclopedia of Materials: Science and Technology pages 1–6 (2001).

[7] E. H. Hwang and S. Das Sarma, Phys. Rev. B 75, 205418 (2007).

[8] A Yu Nikitin, F Guinea, Francisco J Garcia-Vidal, and Luis Martin-Moreno, Physical Review B 85(8), 081405 (2012).

[9] Zheyu Fang, Yumin Wang, Zheng Liu, Andrea Schlather, Pulickel M Ajayan, Frank HL Koppens, Peter Nordlander, and Naomi J Halas, Acs Nano 6(11), 10222–10228 (2012).

[10] Bing Wang, Xiang Zhang, Xiaocong Yuan, and Jinghua Teng, Applied Physics Letters 100(13), 131111 (2012).

[11] AA Dubinov, V Ya Aleshkin, V Mitin, T Otsuji, and V Ryzhii, Journal of Physics: Condensed Matter 23(14), 145302 (2011).

[12] Xiaoguang Luo, Teng Qiu, Weibing Lu, and Zhenhua Ni, Materials Science and Engineering: R: Reports 74(11), 351–376 (2013).

[13] M. Jablan, H. Buljan, Y. Yin, and M Soljačić, Phys. Rev. B 80(24), 245435 (2009).

[14] AC Ferrari, JC Meyer, V Scardaci, C Casiraghi, Michele Lazzeri, Francesco Mauri, S Piscanec, Da Jiang, KS Novoselov, S Roth, et al., Physical review letters 97(18), 187401 (2006).

[15] J Maultzsch, S Reich, C Thomsen, H Requardt, and P Ordejón, Physical review letters 92(7), 075501 (2004).

[16] Fang Liu, Pingbing Ming, and Ju Li, Physical Review B 76(6), 064120 (2007).

[17] Luis Brey and HA Fertig, Physical Review B 75(12), 125434 (2007).

[18] Yurii E Lozovik and Alexey A Sokolik, Nanoscale research letters 7(1), 1–10 (2012).

[19] Kun Yang, S Das Sarma, and AH MacDonald, Physical Review B 74(7), 075423 (2006).

[20] Tsung-Ta Tang, Yuanbo Zhang, Cheol-Hwan Park, Baisong Geng, Caglar Girit, Zhao Hao, Michael C Martin, Alex Zettl, Michael F Crommie, Steven G Louie, et al., Nature nanotechnology 5(1), 32–36 (2010).

[21] C. Kittel, in Introduction to Solid State Physics, 1st ed., (John Wiley and Sons, New York, NY, 1953).

[22] Gabriele Giuliani and Giovanni Vignale, , 2005).

[23] Radi A Jishi, Feynman diagram techniques in condensed matter physics (Cambridge University Press, New York, 2013).

[24] H Bruus K Flensberg and H Bruus, Many-body quantum theory in condensed matter physics (Oxford University Press New York, Oxford, 2004).

[25] Alexander L Fetter and John Dirk Walecka, Quantum theory of many-particle systems (Courier Corporation, Mineola, 2003).

[26] B. Wunsch, T. Stauber, F. Sols, and F Guinea, New Journal of Physics 8 (2006).

[27] RR Nair, P Blake, AN Grigorenko, KS Novoselov, TJ Booth, T Stauber, NMR Peres, and AK Geim, Science 320(5881), 1308–1308 (2008).

[28] Francesco Bonaccorso, Z Sun, T Hasan, and AC Ferrari, Nature photonics 4(9), 611–622 (2010).

[29] Ray Egerton, , 2011).

[30] C Kramberger, R Hambach, C Giorgetti, MH Rümmeli, M Knupfer, J Fink, B Büchner, Lucia Reining, E Einarsson, S Maruyama, et al., Physical review letters 100(19), 196803 (2008).

[31] T Eberlein, U Bangert, RR Nair, R Jones, M Gass, AL Bleloch, KS Novoselov, A Geim, and PR Briddon, Physical Review B 77(23), 233406 (2008).

[32] Junbo Wu, Mukul Agrawal, Héctor A Becerril, Zhenan Bao, Zunfeng Liu, Yongsheng Chen, and Peter Peumans, ACS nano 4(1), 43–48 (2009).

[33] Tae-Hee Han, Youngbin Lee, Mi-Ri Choi, Seong-Hoon Woo, Sang-Hoon Bae, Byung Hee Hong, Jong-Hyun Ahn, and Tae-Woo Lee, Nature Photonics 6(2), 105–110 (2012).

[34] Gunho Jo, Minhyeok Choe, Sangchul Lee, Woojin Park, Yung Ho Kahng, and Takhee Lee, Nanotechnology 23(11), 112001 (2012).

[35] Sukang Bae, Hyeongkeun Kim, Youngbin Lee, Xiangfan Xu, Jae-Sung Park, Yi Zheng, Jayakumar Balakrishnan, Tian Lei, Hye Ri Kim, Young Il Song, et al., Nature nanotechnology 5(8), 574–578 (2010).

[36] Sukosin Thongrattanasiri, Frank HL Koppens, and F Javier García de Abajo, Physical review letters 108(4), 047401 (2012).

[37] Jessica R Piper and Shanhui Fan, ACS Photonics 1(4), 347–353 (2014).

[38] Stefan Alexander Maier, Plasmonics: fundamentals and applications: fundamentals and applications (Springer Science & Business Media, Bath, 2007).

[39] William L Barnes, Alain Dereux, and Thomas W Ebbesen, Nature 424(6950), 824–830 (2003).

[40] RH Ritchie, Physical Review 106(5), 874 (1957).

[41] CJ Powell and JB Swan, Physical Review 115(4), 869 (1959).

[42] Lin Chen, Xun Li, Guoping Wang, Wei Li, Sihai Chen, Long Xiao, and Dingshan Gao, Lightwave Technology, Journal of 30(1), 163–168 (2012).

[43] Amanda J. Haes and Richard P. Van Duyne, Journal of the American Chemical Society 124(35), 10596–10604 (2002). PMID: 12197762.

[44] Ekmel Ozbay, science 311(5758), 189–193 (2006).

[45] Stefan A Maier, Mark L Brongersma, Pieter G Kik, Scheffer Meltzer, Ari AG Requicha, and Harry A Atwater, Advanced Materials 13(19), 1501–1505 (2001).

[46] JM Pitarke, VM Silkin, EV Chulkov, and PM Echenique, Reports on progress in physics 70(1), 1 (2007).

[47] Alessandro Principi, Giovanni Vignale, Matteo Carrega, and Marco Polini, Physical Review B 88(19), 195405 (2013).

[48] AN Grigorenko, Marco Polini, and KS Novoselov, Nature photonics 6(11), 749–758 (2012).

[49] F. H. L. Koppens, D. E. Chang, and F. J. G Abajo, Nano Letters pages 3370–3377 (2011).

[50] Michele Tamagnone, JS Gomez-Diaz, Juan Ramon Mosig, and Julien Perruisseau-Carrier, Applied Physics Letters 101(21), 214102 (2012).

[51] Ashkan Vakil and Nader Engheta, Science 332(6035), 1291–1294 (2011).

[52] Y. Saito, Y. Tani, N. Miyagawa, K. Mitsushima, A. Kasuya, and Y. Nishina, Chem. Phys. Lett. 294, 593–598 (1998).

[53] Ken-ichi Sasaki, Keiko Kato, Yasuhiro Tokura, Satoru Suzuki, and Tetsuomi Sogawa, Physical Review B 86(20), 201403 (2012).

[54] H. Bruss and K. Flensberg, in Many-Body Quantum Theory in Condensed Matter Physics, (Oxford University Press, Oxford, New York, 2004).

[55] A. Ferreira, J. V. Gomes, Y. V. Bludov, P. Pereira, N. M. R. Peres, and A. H. C. Neto, Phys. Rev. B 84, 235410 (2011).

[56] K. S. Novoselov et al., Nature 438, 197 (2005).

[57] R. Saito, K. Sato, P.T. Araujo, D.L. Mafra, and M.S. Dresselhaus, Solid State Communications 175-176, 18–34 (2013).

[58] G Gómez-Santos and T Stauber, EPL (Europhysics Letters) 99(2), 27006 (2012).